Clinical Neurophysiology 171 (2025) 164–181

Contents lists available at ScienceDirect

Clinical Neurophysiology

journal homepage: www.elsevier.com/locate/clinph

Abnormal electroencephalographic rhythms from quiet wakefulness to light sleep in Alzheimer's disease patients with mild cognitive impairment

Enrico Michele Salamone [a,1], Matteo Carpi [a,1], Giuseppe Noce [b], Claudio Del Percio [a], Susanna Lopez [a], Roberta Lizio [a], Dharmendra Jakhar [a], Ali Eldellaa [a], Veronica Henao Isaza [a], Burcu Bölükbaş [a,c], Andrea Soricelli [b,d], Marco Salvatore [d], Bahar Güntekin [c], Görsev Yener [e,f], Federico Massa [g,h], Dario Arnaldi [g,i], Francesco Famà [g,i], Matteo Pardini [g,h], Raffaele Ferri [j], Michele Salemi [j], Bartolo Lanuzza [j], Fabrizio Stocchi [k], Laura Vacca [k], Chiara Coletti [k], Moira Marizzoni [l], John Paul Taylor [m], Lutfu Hanoğlu [n], Nesrin Helvacı Yılmaz [o], İlayda Kıyı [p], Hilal Kula [p], Giovanni B. Frisoni [l,q], Sofia Cuoco [r], Paolo Barone [r], Anita D'Anselmo [s], Laura Bonanni [s], Roberta Biundo [t], Fabrizia D'Antonio [u], Giuseppe Bruno [u], Franco Giubilei [v], Angelo Antonini [t], Claudio Babiloni [a,w,*]

[a] *Department of Physiology and Pharmacology "Vittorio Erspamer", Sapienza University of Rome, Rome, Italy*
[b] *IRCCS Synlab SDN, Naples, Italy*
[c] *Department of Biophysics, School of Medicine, Istanbul Medipol University, Istanbul, Turkey*
[d] *Department of Medical, Movement and Well-being Sciences, University of Naples Parthenope, Naples, Italy*
[e] *Department of Neurology, Faculty of Medicine, Dokuz Eylül University, İzmir, Türkiye*
[f] *IBG: International Biomedicine and Genome Center, Izmir, Turkey*
[g] *Dipartimento di Neuroscienze, Oftalmologia, Genetica, Riabilitazione e Scienze Materno-infantili (DiNOGMI), Università di Genova, Italy*
[h] *Clinica neurologica, IRCCS Ospedale Policlinico San Martino, Genova, Italy*
[i] *Neurofisiopatologia, IRCCS Ospedale Policlinico San Martino, Genova, Italy*
[j] *Oasi Research Institute – IRCCS, Troina, Italy*
[k] *IRCCS San Raffaele, Rome, Italy*
[l] *Laboratory of Alzheimer's Neuroimaging and Epidemiology, IRCCS Istituto Centro San Giovanni di Dio Fatebenefratelli, Brescia, Italy*
[m] *Translational and Clinical Research Institute, Faculty of Medical Sciences, Newcastle University, UK*
[n] *Department of Neurology, School of Medicine, Istanbul Medipol University, Istanbul, Turkey*
[o] *Medipol University Istanbul Parkinson's Disease and Movement Disorders Center (PARMER), Istanbul, Turkey*
[p] *Health Sciences Institute, Department of Neurosciences, Dokuz Eylül University, Izmir, Turkey*
[q] *Memory Clinic and LANVIE – Laboratory of Neuroimaging of Aging, University Hospitals and University of Geneva, Geneva, Switzerland*
[r] *Department of Medicine, Surgery and Dentistry "Scuola Medica Salernitana", Neuroscience Section, University of Salerno, Baronissi, Italy*
[s] *Department of Aging Medicine and Sciences, University "G. d'Annunzio" of Chieti-Pescara, Italy*
[t] *Department of Neuroscience, University of Padua, Padua (PD), Italy*
[u] *Department of Human Neurosciences, Sapienza University of Rome, Rome, Italy*
[v] *Department of Neuroscience, Mental Health, and Sensory Organs, Sapienza University of Rome, Rome, Italy*
[w] *Hospital San Raffaele Cassino, Cassino (FR), Italy*

ARTICLE INFO

Keywords:
Quiet wakefulness
Excessive daytime sleepiness (EDS)
Vigilance dysfunctions
Alzheimer's disease (AD)
Mild cognitive impairment (MCI)
Dementia
Resting-state Electroencephalographic rhythms

ABSTRACT

Objectives: Alzheimer's disease patients with mild cognitive impairment (ADMCI) show abnormal resting-state eyes-closed electroencephalographic (rsEEG) alpha rhythms (8–12 Hz) and may suffer from daytime sleepiness. Our exploratory study tested the hypothesis that they may present characteristic EEG rhythms from quiet wakefulness to light sleep during diurnal recordings.
Methods: Datasets of 34 ADMCI and 22 matched healthy elderly (Nold) subjects were obtained from international archives. EEG recordings lasted approximately 30 min. Transitions of EEG activity from quiet wakefulness

* Corresponding author at: Department of Physiology and Pharmacology "V. Erspamer", Sapienza University of Rome, P. le A. Moro 5, 00185, Rome, Italy.
E-mail address: claudio.babiloni@uniroma1.it (C. Babiloni).
[1] Equally contributing authors.

https://doi.org/10.1016/j.clinph.2025.01.012
Accepted 22 January 2025
Available online 31 January 2025

(EEG)
Delta and alpha rhythms

(alpha-dominant) to light sleep (theta-dominant ripples) were scored according to Hori's vigilance stages. Cortical source activities were computed using the eLORETA software.
Results: ADMCI (t-ADMCI, N = 18) over Nold (t-Nold, N = 11) participants were characterized by greater frontal EEG delta source activities and a lesser reduction (reactivity) in the posterior alpha source activities from quiet wakefulness to ripples. Notably, EEG delta source activities during quiet wakefulness were also greater in the ADMCI group transitioning to light sleep as compared to patients without said vigilance reduction.
Conclusions: These results suggest that ADMCI patients with a greater susceptibility to daytime sleepiness may show characteristic EEG delta and alpha rhythms in the transition from quiet vigilance to daytime sleep.
Significance: Our study showed a derangement of EEG rhythms during the transition to sleep possibly specific to AD.

1. Introduction

Alzheimer's disease (AD) is the most common neurodegenerative disorder associated with aging, accounting for a substantial proportion of dementia cases worldwide. According to the World Alzheimer Report 2018 (https://www.alzint.org/resource/world-alzheimer-report-2018/), AD affects over 30 million people globally, with this number projected to double by 2050. The pathological hallmarks of AD include extracellular amyloid-beta plaques and intraneuronal inclusions of misfolded phospho-tau (p-tau) proteins. Current international guidelines for the clinical assessment of AD patients focus on evaluating cognitive deficits using neuropsychological tests and clinical scales, covering stages from mild cognitive impairment (ADMCI) to dementia (ADD) (Jack et al., 2024, 2018). The etiological diagnosis involves assessing brain amyloidosis and tauopathy through fluid biomarkers (CSF or blood plasma) or neuroimaging (PET) (Jack et al., 2024, 2018). Additionally, structural MRI (sMRI) is used to monitor brain neurodegeneration throughout the disease progression (Jack et al., 2024, 2018).

Despite these well-established clinical guidelines, a frequently overlooked yet clinically significant manifestation of AD is the dysregulation of consciousness-vigilance levels, characterized by excessive daytime sleepiness and frequent, prolonged naps (Babiloni et al., 2020a). This dysregulation has been linked to cerebral amyloid deposition (Lim et al., 2014), cognitive decline (Lim et al., 2013), and functional impairments (Moran et al., 2005). Furthermore, excessive daytime sleepiness has been identified as a predictor of dementia onset (Leng et al., 2019; Li et al., 2023), while short naps (<30 min) have been associated with cognitive benefits (Kitamura et al., 2021; Lovato and Lack, 2010; Pengsuwankasem et al., 2023).

This dysregulation in vigilance can severely impact the quality of life of ADMCI and ADD patients by disrupting daily activities, such as watching television or reading. Identifying biomarkers to assess this dysfunction is crucial for evaluating treatment efficacy in these patients. Resting-state EEG (rsEEG) offers an ideal biomarker for this purpose, as it is non-invasive, cost-effective, and easily repeatable, without concerns for *meta*-learning effects. In cognitively unimpaired older (Nold) people, rsEEG is characterized by prominent alpha rhythms (8–12 Hz) in parietal and occipital regions during quiet wakefulness and transient high-frequency (>16 Hz) activity during cognitive or motor tasks (Babiloni et al., 2020a). Compared to those people, rsEEG analyses in AD patients have revealed several abnormalities: (1) increased delta (< 4 Hz) and theta (4–7 Hz) power and interdependence between electrode or source pairs; (2) slowing in frequencies of the rsEEG alpha rhythms with a mean power peak in the alpha range at 8 Hz or lower in comparison with 9 Hz or higher typically observed in cognitively unimpaired older people, thus suggesting the need of an individually-based determination of alpha frequency band in ADD and ADMCI patients (Babiloni et al., 2020a); (3) decreased alpha power in posterior scalp regions, indicating cortical hyperexcitability; (3) high accuracy (> 80 %) in discriminating ADMCI and ADD patients from controls; and (4) progressive worsening of these abnormalities over 12–24 months, with some evidence of improvement following cholinergic treatment (Babiloni et al., 2020b; Rossini et al., 2020).

These findings indicate that spectral rsEEG measures are reliable indicators of dysregulated neurophysiological mechanisms responsible for maintaining vigilance in ADMCI and ADD patients, both at group and individual levels. Based on these observations, we propose a novel hypothesis: the transition from quiet wakefulness to light non-rapid eye movement (NREM) sleep, a key period of arousal regulation, may be abnormal in ADMCI patients, reflecting dysfunctions in subcortical systems responsible for promoting wakefulness.

A promising model to explore these neurophysiological mechanisms has been applied in studies of patients with major depression and insomnia, where continuous EEG recordings for 30 min revealed hyperstable brain arousal and persistent alpha rhythms during relaxation (Losert et al., 2020; Schmidt et al., 2017; Ulke et al., 2019). Similarly, magnetoencephalographic (MEG) recordings in Nold participants demonstrated transitions from dominant alpha rhythms to widespread delta and theta rhythms during light NREM sleep (Fan et al., 2023). Building on these findings, the present study aims to test the novel hypothesis that ADMCI patients, compared to Nold participants, exhibit abnormal delta and theta EEG rhythms during the transition from quiet wakefulness to light NREM sleep in diurnal EEG recordings lasting approximately 30 min. This investigation offers a novel approach to understanding vigilance dysfunctions in ADMCI patients. It provides clinically relevant insights into the neurophysiological underpinnings of excessive daytime sleepiness in the prodromal stages of AD. The study also highlights the potential for incorporating EEG measures into the clinical assessment of ADMCI and ADD patients to account for this often neglected yet significant dimension of the disease.

2. Materials and methods

2.1. Participants and diagnostic criteria based on clinical measures and biomarkers

The present exploratory EEG study is unique in applying Hori's staging criteria (Hori et al., 1994) to analyze EEG markers of vigilance transitions—from quiet vigilance to Flattening and Ripples—in ADMCI patients compared to matched Nold controls. Given this novelty, it was not possible to base our sample size calculations on previous studies utilizing these specific markers. As an approximation, we based the power analysis on the hypothesis that significant differences would be detected between ADMCI and Nold groups in occipital rsEEG alpha source activity, as demonstrated in prior research (Babiloni et al., 2021a, 2021b).

Specifically, the sample size was determined using a-priori power analysis, targeting a minimum statistical power of 0.80 with a significance level of 0.05. We conducted this analysis with G*Power 3.1.9.7 (https://gpower.software.informer.com/3.1/), referencing past studies from the PDWAVES Consortium (www.pdwaves.eu) on resting-state EEG markers in ADMCI patients published in peer-reviewed journals. To inform these calculations, we used the partial eta-squared effect size from multivariate ANOVA results in a related study (Babiloni et al., 2018a), which investigated EEG abnormalities in MCI patients due to Alzheimer's and Lewy body diseases, applying similar clinical and EEG methodologies with non-overlapping datasets.

In G*Power, we conducted an a-priori power analysis within the F-test family, selecting the repeated measures ANOVA with a within-between-factor interaction option. We computed the partial eta-squared for the Group X Band interaction in an ANOVA design with two groups (ADMCI vs. Nold) and occipital rsEEG alpha source activities (i.e., alpha 1 occipital, alpha 2 occipital, and alpha 3 occipital), obtaining a value of 0.308, corresponding to a Cohen's f effect size of 0.667. Based on this estimate, G*Power suggested a sample size of 24 subjects for an ANOVA design with 3 measures (rsEEG occipital alpha 1, 2, and 3 source activities) and the 2 groups (ADMCI vs. Nold). The analysis suggested a sample size of N = 25 per group, providing an empirical basis for the present exploratory study.

The Partners and institutional affiliations of the PDWAVES Consortium and the PharmaCog project contributing to this study are reported on the cover page of this manuscript. The datasets used were formed by clinical, neuropsychological, anthropometric, genetic, CSF, sMRI, and rsEEG markers obtained in 34 ADMCI patients and 22 Nold seniors as controls (see Table 1).

These Nold and ADMCI participants were recruited by the following Italian and Turkish clinical units of the PDWAVES Consortium: the Sapienza University of Rome (Italy), the IRCCS Institute for Research and Evidence-based Care (IRCCS) "Fatebenefratelli" of Brescia (Italy), the IRCCS Synlab SDN of Naples (Italy), the Oasi Research Institute-IRCCS, Troina (Italy), the IRCCS Ospedale Policlinico San Martino and DINOGMI (University of Genova, Italy), the IRCCS San Raffaele Pisana of Rome (Italy), Dokuz Eylül University (Turkey), and the Medipol University of Istanbul (Turkey).

Local institutional Ethics Committees approved the present observational study. All experiments were performed with the informed consent of each participant in accordance with the Code of Ethics of the World Medical Association (Declaration of Helsinki) and the standards of the local Institutional Review Board.

The diagnosis of AD in the ADMCI patients was based on the "positivity" for the Aβ1-42/phospho-tau ratio (Aβ42/p-tau) in the CSF biomarker or MRI evidence of neurodegeneration in the typical neuroanatomical targets of the disease in the hippocampus, temporoparietal junction, precuneus, and posterior cingulate regions (Albert et al., 2011). The local physicians in charge judged the "positivity" for releasing the clinical diagnosis of "AD" to the patients, according to the local diagnostic routine of the participating clinical Units.

The clinical inclusion criteria for ADMCI patients were as follows: (1) age of 55–90 years; (2) reported memory complaints by the patient and a relative; (3) a Mini-Mental State Examination (MMSE; Folstein et al., 1975) score of 24 or higher; (4) Clinical Dementia Rating (CDR; Morris, 1993) score of 0.5; (5) logical or verbal memory test score of 1.5 standard deviations (SD) below the mean adjusted for age (Schmidt, 1996; Wechsler, 1987); the cognitive deficits must not significantly impair functional independence in activities of the daily living; (6) 30-item Geriatric Depression Scale (GDS; Yesavage et al., 1982) score of 5 or less; (7) modified Hachinski Ischemic Score (HIS; Rosen et al., 1980) of 4 or less and educational attainment of 5 years or more; and (8) single- or multi-domain amnesic MCI status.

The clinical exclusion criteria for ADMCI patients were as follows: (1) significant systemic and neurological illness; (2) major psychiatric diseases, including a history of drug use, alcohol use, and other cases under a substance use disorder according to DSM-5. Specifically, this disorder involves patterns of symptoms caused by using a substance that an individual continues taking despite its negative effects); (3) any diseases belonging to dementia or mixed dementia; (4) current participation in a clinical trial using disease-modifying drugs; (5) systematic use of antidepressants with anticholinergic side effects; (6) chronic use of neuroleptics, narcotics, analgesics, sedatives or hypnotics; (7) anti-parkinsonian medications (cholinesterase inhibitors and memantine allowed); (8) diagnosis of epilepsy or history of seizures or epileptiform EEG signatures, and (9) major depressive disorder as described in the Diagnostic and Statistical Manual of Mental Disorders (DSM-5; American Psychiatric Association, 2013).

In all ADMCI patients, AD-relevant CSF biomarkers were assessed in a neurobiological definition of AD according to the NIA-AA Research Framework (Albert et al., 2011; Jack et al., 2018). The CSF samples were pre-processed, frozen, and stored in accordance with the Alzheimer's Association Quality Control Programme for CSF biomarkers (Mattsson, 2011). Dedicated single-parameter colorimetric enzyme-linked immunosorbent assay ELISA kits (Innogenetics, Ghent, Belgium) were used to measure amyloid beta 1–42 (i.e., Aβ42). Levels of the protein tau (i.e., total tau, t-tau) and a phosphorylated form of tau at residue 181 (i.e., p-tau) were also measured. Assays were performed in parallel from a frozen aliquot of CSF according to the manufacturer's instructions. Each sample was assayed in duplicate. A sigmoidal standard curve was plotted to allow the quantitative expression (pg/ml $^{-1}$) of the measured light absorbance. All ADMCI patients in the present study were "positive" for the CSF Aβ42/p-tau biomarker at a threshold defined in a previous investigation by our working group (Marizzoni et al., 2020). In that investigation, the cut-off for "positivity" for that CSF Aβ42/p-tau biomarker was 15.2 for *APOE* e4 (*APOE4)* carriers and 8.9 for *APOE4* non-carriers (Marizzoni et al., 2020). In the present study, all ADMCI patients with *APOE4* status had CSF Aβ42/p-tau lower than 15.2, whereas the ADMCI patients without *APOE* status had CSF Aβ42/p-tau lower than 8.9.

Table 2 reports the clinical, genetic, and CSF data relevant to

Table 1
Mean ± SE of demographic information and clinical characteristics of the ADMCI and Nold samples. *Legend*: ADMCI: participants with mild cognitive impairment due to Alzheimer's disease; Nold: cognitively normal older participants; GDS: Geriatric Depression Scale; MMSE: Mini-Mental State Examination; TF: transition frequency; IAFp: individual alpha frequency peak.

Demographic and clinical data in ADMCI and Nold participants (mean ± SE)		
	ADMCI (N = 34)	**Nold (N = 22)**
Age	71.0 ± 1.0	65.6 ± 8.5
Sex [M/F (% M)]	15/19 (44.1 %)	10/12 (45.5 %)
Education	12.1 ± 0.8	14.7 ± 0.8
GDS [a]	3.0 ± 0.4	2.6 ± 0.7
MMSE	26.0 ± 0.5	29.8 ± 0.1
TF	5.4 ± 0.2	5.9 ± 0.2
IAFp	8.8 ± 0.3	9.6 ± 0.3

[a] : The GDS score was not available for 4 t-Nold participants; hence, the mean was obtained on 18 subjects.

Table 2
Mean ± SE of clinical data, genotype, and cerebrospinal fluid biomarkers in ADMCI participants. *Legend:* ADMCI: participants with mild cognitive impairment due to Alzheimer's disease; GDS: Geriatric Depression Scale; MMSE: Mini-Mental State Examination.

Demographic data, clinical data, genotype, and biomarkers in ADMCI participants (mean ± SE)	
	ADMCI (N = 34)
GDS	3.0 ± 0.4
CDR	0.5 ± 0.0
HIS [a]	0.7 ± 0.1
APOE-ε4 [b]	25/6 (80.5 %)
Amyloid-β [b]	531.7 ± 18.8
Total Tau [b]	573.7 ± 51.2
P-Tau [b]	82.5 ± 6.2
Amyloid-β/P-Tau [b]	7.6 ± 0.6

[a] : HIS was not available for 3 ADMCI participants, hence the mean was obtained on 31 subjects.

[b] : Genotype and fluid biomarkers were not obtained for 3 ADMCI participants, hence these data refer to 31 ADMCI subjects.

characterize the ADMCI group for future cross-validation studies. Specifically, the mean scores (± standard error of the mean, SE) of GDS, CDR, and modified HIS are reported. The mean percentage of *APOE* genetic risk for AD and the mean group values of CSF p-tau (pg/ml), t-tau (pg/ml), and Aβ42/p-tau diagnostic biomarkers for AD are also reported.

Furthermore, relevant sMRI markers were measured in all ADMCI patients. All sMRI scans were performed with a 3.0 Tesla scanner. The sMRI protocol consisted of several acquisitions, including two T1-weighted, anatomical T2-weighted fluid-attenuated inversion recovery (FLAIR), and diffusion tensor imaging (DTI) scans.

In the centralized analysis of the sMRIs, all data were visually inspected for quality assurance prior to extraction of the MRI biomarkers. Specifically, we checked that there were no gross partial brain coverage errors or major visible artifacts, including motion, wrap-around, radio frequency interference, and signal intensity or contrast inhomogeneities. The two anatomical T1-weighted sMRI scans were averaged. Data were analysed using FreeSurfer version 5.1.0 to automatically generate: (1) volumes of the total gray matter, total white matter, caudate nucleus, putamen nucleus, globus pallidus, nucleus accumbens, hippocampus, amygdala, and lateral ventricle; (2) total cortical thickness of the entorhinal cortex; and (3) white matter hypointensity (Desikan et al., 2006; Fischl et al., 2004). Those volumes were normalized to the total intracranial volume (TIV). In addition, the T2-weighted FLAIR MRI scans were analysed using the FMRIB Software Library (FSL) version 5.0.3 to evaluate the subcortical white matter lesions to control for the AD diagnosis.

A detailed description of the acquisition and analysis of the DTI MRI data is reported by Jovicich and colleagues (2014) and is only sketched here. The automated quality control of the diffusion MRI data was performed by the DTIPrep tool. It applied motion and other corrections to those data. The post-processing was performed using FSL for skull and non-brain tissue removal (BET). FSL was also used to estimate the standard diffusion biomarkers, such as fractional anisotropy (FA), mean diffusivity (MD), axial diffusivity (AxD), and radial diffusivity (RD). The analysis explored several of the brain's white matter tracts mentioned in the following paragraphs. These tracts were predefined in the Johns Hopkins University ICBM-FA-1 mm atlas and were back-projected with a nonlinear co-registration to FA, MD, AxD, and RD maps on track-based spatial statistics space for each ADMCI participant (Smith et al., 2006).

Anthropometric features (e.g., weight, height, and body mass index) and cardiovascular markers (e.g., systolic blood pressure, diastolic blood pressure, pulse pressure, mean arterial pressure and heart rate) were also measured as control variables for diagnostic purposes.

All ADMCI patients were assessed for their global cognitive status and performance in several cognitive domains, including memory, language, executive function, planning, visuospatial function, and attention, were assessed. All ADMCI patients showed a significant decline in performance on at least one episodic memory test, which in most cases was associated with a significant decline in the performance on neuropsychological tests assessing other cognitive domains. In the following, we report the cognitive domains investigated and the neuropsychological tests administered to the ADMCI patients: (1) global cognitive status was assessed using the MMSE and the Alzheimer's Disease Assessment Scale – Cognitive Subscale (ADAS-Cog; Rosen et al., 1984); (2) episodic memory was assessed by the immediate and delayed recall of the Rey Auditory Verbal Learning Test (Schmidt, 1996); (3) executive functions and attention were assessed by the Trail Making Test (TMT) Parts A and B (Reitan and Wolfson, 1985); (4) language was assessed by the 1-minute Verbal Fluency Test for Letters and 1-minute Verbal Fluency Test for Categories (fruits, animals or car trades; Novelli et al., 1986); and (5) planning abilities and visuospatial functions were assessed by the Clock Drawing and Copy Test (Freedman et al., 1994).

All Nold seniors underwent an interview and cognitive screening (including MMSE and GDS) and physical and neurological examinations to exclude subjective memory complaints (SMC), cognitive deficits, and mood disorders. All Nold seniors had an MMSE score $\geq$ 27, a CDR score equal to 0, and a GDS score below the threshold of 5 (no depression) or were assessed as having no depression after an interview with a physician or a clinical psychologist at the time of the enrollment. Nold seniors with a history of past or present neurological or psychiatric illness were also excluded. In addition, Nold seniors affected by any chronic systemic disease (e.g., diabetes mellitus) were excluded, as were Nold seniors who were chronically taking psychoactive drugs. Unfortunately, sMRI, CSF, and *APOE* genotyping were not available for the present Nold seniors.

2.2. The electroencephalographic (EEG) recordings

EEG recordings were performed in the morning to minimize fatigue and sleep pressure effects. Participants took their eventual psychotropic drugs after the EEG recording. They were not asked for a complete drug washout for obvious ethical reasons. Rather, this procedure made the EEG recordings in the ADMCI patient group comparable in terms of drug status.

The rsEEG activity was recorded while the participants were seated on a comfortable reclined chair in a quiet room with dim lighting. There were three recording conditions: (1) ***Resting-state eyes closed***, lasting 3–5 min as a function of the quality of the EEG recording; (2) ***Resting-state eyes open***, lasting 3–5 min as a function of the quality of the EEG recording; and (3) ***Vigilance***, lasting approximately 30 min. Before the first condition, the experimenters gave the participants the instructions. In the instructions, the three conditions mentioned above were introduced. During the first two conditions, the participants were encouraged to experience quiet wakefulness with muscle relaxation and no voluntary movements, talking, or systematic goal-oriented mentalization. They were also informed that if they showed behavioral or EEG signs of drowsiness, the experimenters would kindly warn them to return to the quiet wakefulness mode. In contrast to the first two conditions, the third condition (Vigilance) was designed to leave participants free to sleep without receiving any alert until the end of the recording.

Each clinical unit used its local EEG recording setting to avoid aliasing phenomena. Some clinical units used 0.01–60 Hz of analog bandpass filter and 128 Hz frequency sampling, while others used 0.01–100 Hz of analog bandpass filter and 256 or 516 Hz frequency sampling. This setting avoided aliasing and is suitable for testing the present working hypothesis on the transition from quiet vigilance to light sleep during EEG recordings, which is focused on EEG delta ($<$ 4 Hz), theta (4–7 Hz), and alpha (8–12 Hz) rhythms. Notably, the 128 Hz frequency sampling allowed the evaluation of EEG activity from 13 to 60 Hz to control for the expected progressive reduction of EEG power density with the increase in frequencies when EEG data are free from significant electromyographic artifacts due to excessive muscle tension of facial and neck muscles.

The electrode montage included 19 scalp monopolar sensors placed according to the 10–20 system (i.e., O1, O2, P3, Pz, P4, T3, T5, T4, T6, C3, Cz, C4, F7, F3, Fz, F4, F8, Fp1, and Fp2). A frontal ground electrode was typically used, while cephalic or linked earlobe electrodes were used as electrical references according to local methodological facilities and standards. Electrode impedances were kept below 5 kΩ. Vertical and horizontal electro-oculographic (EOG) potentials (0.3–70 Hz band-pass) were recorded using the same EEG settings to control eye movements and blinking.

During the first two conditions (i.e., the two Resting-state conditions), the experimenters paid special attention to detecting rsEEG activity with signs of sleep intrusion, such as a ***flattening*** of the amplitude of posterior rsEEG alpha rhythms during the rsEEG recording and a progressive amplitude increase of ***ripples*** (rsEEG theta rhythms), eventually followed by vertex shape waves, K complexes, sleep spindles, and slow waves. In those moments, they alerted the participants to stay awake and take note of them. (e.g., report of participant's drowsiness, open eyes, arm/hand movements, etc.).

2.3. The preliminary EEG data analysis

The recorded EEG activity was centrally analyzed by the experts of the Department of Physiology and Pharmacology (V. Erspamer) of the Sapienza University of Rome (C.D.P., G.N., E.M.S., M.C., and S.L.). They have been involved for years in visual and spectral analysis of rsEEG rhythms in Nold or MCI individuals. Therefore, they know well the general features of these rhythms and could recognize if a given EEG dataset belonged to Nold or MCI individuals. To prevent the potential effects of this implicit knowledge as a source of variability in the EEG classification, we informed all raters about the clinical diagnosis associated with the EEG datasets to be analyzed in this study (i.e., Nold or ADMCI).

The analysis to detect and remove the artifacts from the recorded EEG activity followed the same procedures used in previous EEG studies in ADMCI patients by the PDWAVES Consortium (Babiloni et al., 2018b, 2017) to compare the results across the various studies. For this reason, it will be only summarized below.

EEG data were exported as European data format (.edf) or EEGLAB set (.set) files and then processed offline using the EEGLAB toolbox (version eeglab14_1_2b; Delorme and Makeig, 2004) running under the MATLAB software (MathWorks, Natick, MA, USA; version: R2014b).

The EEG data were then analyzed according to a three-step procedure aimed at detecting and removing (1) any recording channels (electrodes) showing a prolonged artefactual rsEEG activity due to bad electric contacts or other reasons; (2) rsEEG epochs with artifacts in multiple recording channels; and (3) intrinsic components of the rsEEG epochs with artifacts.

The first step was based on a visual analysis of the recorded EEG activity by two independent experimenters among the experts above for a first identification of the selected electrodes affected by irreparable artifacts. In case of a contrasting decision, the case was discussed with a third expert. The final decision was taken based on the concordant decision of 2 of them. These are subjective decisions based on expertise, representing potential sources of variability among raters. However, this kind of expert decision-making process is common in all EEG studies based on visual analysis for the detection of artifacts by trained neurophysiologists. The PDWAVES Consortium opted for this traditional procedure, as there is no international consensus on fully automated procedures for EEG artifact detection and removal in clinical studies, according to an expert panel of the International Federation of Clinical Neurophysiology (Babiloni et al., 2020a).

In the first step of the analysis, no more than 3 selected electrodes of the 10–20 system were removed for each participant. For the clinical units with a digital EEG system with > 19 exploring electrodes, the removed electrodes were replaced by the closest electrodes not included in the 19 electrodes of the 10–20 system. The added electrodes were then used together with the artifact-free selected electrodes to compute the interpolation of artifact-free EEG data to reconstruct the EEG data at the removed electrodes of the 10–20 system through the EEGLAB toolbox, ensuring that all participants had artifact-free EEG data at the locations of those 19 electrodes. Notably, the interpolation technique may introduce a source of variance in the EEG datasets, so we performed a control analysis comparing the mean number of interpolated electrodes between the Nold and ADMCI groups ($p < 0.05$). No statistical difference was observed ($p > 0.05$).

The second step was based on a visual analysis of the recorded EEG activity by three experts among those involved in the operation (i.e., C.D.P., G.N., and S.L.) to develop a first identification of the artefactual EEG epochs. The EEG epochs contaminated by muscular, ocular, head movements, or non-physiological artifacts were digitally annotated by windowing the EEG traces.

The third step was implemented by an independent component analysis (ICA) from the EEGLAB toolbox, which was applied to remove the ICA components representing the residual artifacts due to the following causes: (1) blinking and eye movements; (2) involuntary head movements; (3) neck and shoulder muscle tension; and (4) electrocardiographic activity (Crespo-Garcia et al., 2008; Jung et al., 2000). In this step, the EEG experts performed a visual analysis of the independent components to detect and remove those showing the typical pattern of eye movements, saccades, heartbeats, and electromyographic activity due to excessive head muscle tensions. Even in this case, we did not find any fully automated procedure that received an international consensus for application in ADMCI patients. For each EEG dataset, less than 5 ICA components were removed from those produced by the EEGLAB toolbox. In this step, the EEG datasets were reconstructed with the remaining (artifact-free) ICA components, and the putative artifact-free EEG epochs were again visually double-checked by two experts to confirm or make the final decision on the inclusion or exclusion of the respective EEG stage.

The artifact-free EEG data were divided into 4-s epochs for further analysis.

2.4. The classification of the artifact-free EEG epochs of the vigilance condition

The analysis of the EEG data investigating the transition from quiet vigilance to light NREM sleep was performed independently by three (i.e., E.M.S., D.J., and M.C.) of the experts above blinded to the diagnosis of the participants. They classified the artifact-free EEG 4-s epochs of the Vigilance condition into three stages, according to a modified version of the classification system outlined by Hori et al. (1994). Prior to this part of the procedure, the three experts critically discussed Hori's classification system. Furthermore, they performed together some classification trials on sample EEG datasets to harmonize the practical application of Hori's criteria to the experimental data. The three stages of the Vigilance condition for the present study are defined below:

(1) ***Wakefulness***, characterized by dominant EEG alpha rhythms at parietal and occipital scalp electrodes for ≥ 75 % of the EEG epoch (i.e., at least 3 s out of the 4-s EEG epoch). This stage corresponds to Hori's stages 1, 2, and 3.

(2) ***Flattening***, characterized by a marked reduction (≥ 50 %) in the amplitude of the EEG alpha rhythms measured in the EEG epochs of the Wakefulness stage. This amplitude reduction must occur in ≥ 75 % of the whole EEG epoch examined.

(3) ***Ripples*** (diffuse theta), characterized by widespread EEG rhythms at the individual theta frequencies that are lower than those marked as EEG alpha rhythms in the Wakefulness stage. Such dominant EEG theta rhythms must occur for ≥ 75 % of the whole EEG epoch examined. This stage corresponds to Hori's stage 5.

All EEG epochs compatible with mixed Vigilance stages were discarded, as well as all EEG epochs with vertex shape waves, K complexes, sleep spindles, and sleep slow waves.

Based on the above classification procedure, each EEG dataset in the Vigilance condition recorded from the Nold or ADMCI participants was classified into two categories: (1) ***Transitional,*** showing at least 30 s (8 EEG epochs) of EEG activity in the Wakefulness stage, at least 30 s of EEG activity in the Flattening stage, and at least 30 s of EEG activity in the Ripples stage and (2) ***Non-transitional,*** due to the lack of EEG activity required for satisfying the above Vigilance stages of Wakefulness, Flattening, and Ripples. Inter-rater variability computed in EEG datasets belonging to two Nold participants and two ADMCI participants resulted in a moderate mean concordance rate of 0.71 (min–max: 0.66–0.76). In all other EEG datasets, any uncertainty on the EEG epochs was managed by a discussion of two raters. If they did not agree on a given classification, the case was resolved by the intervention of a third expert.

The outcome of the above classification procedure was as follows: the EEG datasets classified as Transitional were observed in 18 (t-ADMCI) out of 34 ADMCI patients and in 11 (t-Nold) out of 22 Nold subjects. Table 3 reports the relevant demographic and clinical information (i.e., MMSE score) about the t-Nold and t-ADMCI groups, together with the results of the statistical analyses computed to evaluate

Table 3
Mean ± SE of demographic information and clinical characteristics and results of their statistical comparisons ($p < 0.05$) in t-ADMCI and t-Nold participants. *Legend:* t-ADMCI: participants with mild cognitive impairment due to Alzheimer's disease transitioning into light sleep; t-NOLD: cognitively normal older participants transitioning into light sleep; GDS: Geriatric Depression Scale; MMSE: Mini-Mental State Examination; n.s. = not significant ($p > 0.05$).

Demographic and clinical data in t-ADMCI and Nold participants (mean ± SE)			
	t-ADMCI (N = 18)	**t-Nold (N = 11)**	**Statistical Analysis**
Age	70.0 ± 1.4	65.6 ± 2.6	T-test: n.s.
Sex [M/F (% M)]	7/11 (38.9 %)	3/8 (27.3 %)	Fisher test: n.s.
Education	13.3 ± 1.2	15.8 ± 0.8	T-test: n.s.
GDS [a]	2.8 ± 0.6	1.9 ± 0.4	T-test: n.s.
MMSE	25.9 ± 0.7	29.6 ± 0.3	Mann-Whitney *U* test: $p < 0.001$

[a] : GDS score was not available for 2 t-Nold participants, hence the mean was obtained on 9 subjects.

the presence or absence of statistically significant differences between them as age (*t*-test), sex/gender (Fisher's exact test), education (*t*-test), and MMSE score (Mann-Whitney *U* test). As expected, a statistically significant difference was found between the two groups for the MMSE score ($p = 0.001$), showing a higher score in the Nold than in the ADMCI group. On the contrary, we observed no statistically significant differences in age, gender, and education between the groups ($p > 0.05$).

Table 4
Mean ± SE of demographic data, clinical data, genotype, and cerebrospinal fluid biomarkers and results of their statistical comparisons ($p < 0.05$) in t-ADMCI and nt-ADMCI participants. *Legend:* t-ADMCI: participants with mild cognitive impairment due to Alzheimer's disease transitioning into light sleep; nt-ADMCI: participants with mild cognitive impairment due to Alzheimer's disease not transitioning into light sleep; SES: socioeconomic-status; BMI: body mass index; GDS: Geriatric Depression Scale; MMSE: Mini-Mental State Examination; CDR: Clinical Dementia Rating; HIS: Hachinski Ischemic Score; n.s. = not significant ($p > 0.05$).

Demographic data, clinical data, genotype, and biomarkers in t-ADMCI and nt-ADMCI participants (mean ± SE)			
	t-ADMCI (N = 18)	**nt-ADMCI (N = 16)**	**Statistical Analysis**
Age (years)	70.0 ± 1.4	72.1 ± 1.3	T-test: n.s.
Sex [M/F (% M)]	7/11 (38.9 %)	8/8 (50.0 %)	Fisher test: n.s.
Education (years)	13.3 ± 1.2	10.8 ± 0.9	T-test: n.s.
Living alone [Y/N (% Y)] [a]	0/15 (0 %)	3/13 (18.8 %)	Fisher test: n.s.
SES (low/middle/high)	6/5/5	3/8/4	Chi-square test: n.s
BMI [a]	26.8 ± 0.9	24.7 ± 0.8	T-test: n.s.
GDS	2.8 ± 0.6	3.3 ± 0.6	T-test: n.s.
MMSE	25.9 ± 0.7	26.1 ± 0.6	T-test: n.s.
CDR	0.6 ± 0.1	0.5 ± 0.0	T-test: n.s.
HIS [a]	0.7 ± 0.2	0.6 ± 0.1	T-test: n.s.
Systolic blood pressure (mmHg) [a]	133.6 ± 2.5	135.8 ± 4.0	T-test: n.s.
Diastolic blood pressure (mmHg) [a]	82.9 ± 2.8	75.1 ± 2.5	T-test: n.s.
Heart rate (beats per min) [a]	64.6 ± 2.7	64.8 ± 1.7	T-test: n.s.
Familiarity for dementia [a]	7/8 (46.7 %)	8/8 (50 %)	Fisher test: n.s.
APOE-ε4 [Y/N (% Y)] [b]	12/3 (80.0 %)	13/3 (81.3 %)	Fisher test: n.s.
Amyloid-β [b]	517.7 ± 23.3	544.8 ± 29.5	T-test: n.s.
Total Tau [b]	630.5 ± 87.2	520.6 ± 55.9	T-test: n.s.
P-Tau [b]	89.8 ± 10.2	75.6 ± 7.0	T-test: n.s.
Amyloid-β/P-Tau [b]	6.8 ± 0.8	8.2 ± 0.9	T-test: n.s.

[a] : Data not available for 3 t-ADMCI participants, hence sample size is n = 15.
[b] : Genotype and fluid biomarkers were not obtained for 2 t-ADMCI participants, hence these data refer to 16 t-ADMCI subjects.

Table 4 reports the relevant demographic, clinical, genetic, and CSF data of the t-ADMCI and nt-ADMCI subgroups to characterize them for future cross-validation studies. For the same reasons, the ADMCI patients who received prescriptions for the use of psychoactive drugs as-needed basis are specified in the following. In total, psychoactive drugs were taken by 4 out of 18 t-ADMCI patients (namely Escitalopram N = 3, Duloxetine N = 1, Lormetazepam N = 1) and 8 out of 16 nt-ADMCI patients (Escitalopram N = 3, Duloxetine N = 2, Lormetazepam N = 1, Trazodone N = 2, Zolpidem N = 1). Furthermore, the t-Nold and nt-Nold participants had not received prescriptions for the above psychoactive drugs, so these drugs cannot explain the transitions from quiet wakefulness to light sleep of the t-Nold participants in the present experimental conditions (Table SM1). Given the distribution of that information across participants, we did not use those variables as covariates in statistical models.

Fig. 1 illustrates examples in the t-Nold and t-ADMCI groups of EEG waveforms classified into the three stages of the Vigilance condition (i.e., Wakefulness, Flattening, and Ripples).

2.5. The scalp power density of EEG rhythms

For each participant, the global normalized EEG power density at the scalp electrode level was evaluated. In detail, the procedure was performed as follows: (1) raw EEG data of all clinical units were filtered 0.1–60 Hz. The raw EEG data were then subsampled to 128 Hz if the recording had been performed with sampling frequencies at 256 Hz or 512 Hz. This procedure avoided aliasing and is suitable for testing the present working hypothesis on the transition from quiet vigilance to light sleep during EEG recordings, which is focused on EEG delta (< 4 Hz), theta (4–7 Hz), and alpha (8–12 Hz) rhythms. Furthermore, the evaluation of EEG activity from 13 to 60 Hz allowed us to control for the expected progressive reduction of EEG power density with the increase in frequencies when EEG data are free from significant electromyographic artifacts due to excessive muscle tension of facial and neck muscles; (2) the scalp EEG power density at each electrode and frequency bin was normalized to the mean value obtained by averaging the scalp EEG power density across all frequency bins and scalp electrodes; (3) the global scalp normalized EEG power density at each frequency bin was calculated by averaging the normalized scalp EEG power density values across all 19 electrodes of the 10–20 montage system; and (4) the global scalp normalized EEG power density values at each frequency band of interest were averaged to obtain the frequency band values. Notably, for each participant, the EEG frequency and source analyses of the Wakefulness, Flattening, and Ripple stages were based on all artifact-free EEG epochs classified into the Wakefulness, Flattening, and Ripple stages, respectively.

To control the outcome of the mentioned classification qualitatively, we performed the following procedure. For each Nold and ADMCI participant, we computed the EEG power density across all scalp electrodes for the Wakefulness, Flattening, and Ripple stages separately. Afterward, the grand average of the global EEG power density across all Nold and ADMCI participants was computed for each stage. Supplementary Materials Figure SM1 illustrates the solutions. They clearly show that the EEG power density peak in the alpha frequencies (8–12 Hz) was highest in the Wakefulness state and lowest in the Flattering stage. Furthermore, the EEG power density peak around the theta frequencies (4–6 Hz) was highest in the Ripples stage. These findings agree with what is expected based on the criteria to classify the EEG epochs in the Wakefulness, Flattening, and Ripple stages.

The EEG frequency bands of interest were individually identified using the following frequency landmarks: the rsEEG transition frequency (TF) and the rsEEG individual alpha frequency peak (IAFp; Klimesch, 1999, 1996). In the rsEEG power density spectrum, the TF marks the transition frequency between the theta and alpha bands, defined as the minimum rsEEG power density between 3 and 8 Hz (between the delta and the alpha power peak) in the parietal or occipital

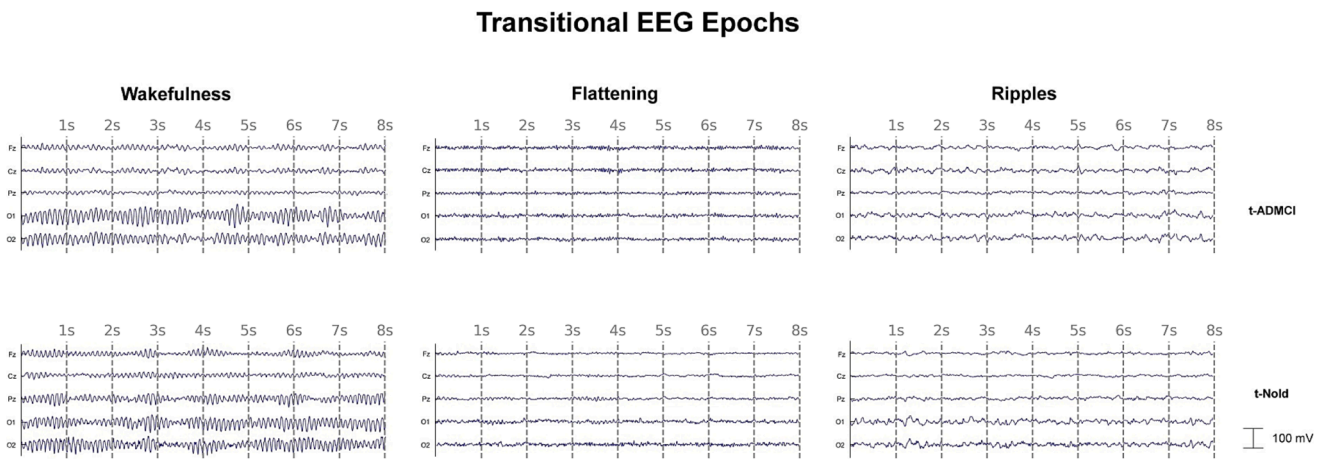

Fig. 1. Example of the three Vigilance Conditions: Wakefulness (Hori Stages 1, 2 and 3), Flattening (Hori Stage 4), Ripples (Hori Stage 5) in two subjects from the t-ADMCI and t-Nold (subjects with Mild Cognitive Impairment due to Alzheimer's Disease and cognitively normal elderly showing transition to light sleep). Each picture represents two 4-seconds epochs of the relevant EEG channels, here depicted in a monopolar montage using the common average as reference, used for scoring the Vigilance Conditions.

scalp electrodes showing alpha power maximum. The IAFp is the maximum rsEEG power density peak between 6 and 14 Hz, typically observed in parietal or occipital electrodes. These frequency landmarks were previously well described by Dr. Wolfgang Klimesch (1996, 1999). The TF and IAFp were computed for each participant included in the study. Based on the TF and IAFp, we estimated the individual EEG delta, theta, and alpha bands as follows: delta from TF −4 Hz to TF −2 Hz, theta from TF −2 Hz to TF, alpha 1 from TF to the frequency midpoint of the TF-IAFp range, alpha 2 from the frequency midpoint of the TF-IAFp range to IAFp, and alpha 3 IAFp to IAFp + 2 Hz.

The other higher frequency bands (i.e., beta and gamma) were not included in the present study based on the lack of significant differences with Nold participants obtained by the research group using the present EEG methodology in ADMCI patients (Babiloni et al., 2021a, 2021b).

2.6. The estimation of EEG cortical sources by low-resolution brain electromagnetic tomography (eLORETA) freeware

We used the official freeware tool, exact low-resolution brain electromagnetic tomography (eLORETA; https://www.uzh.ch/keyinst/loreta.htm), to linearly estimate the cortical source activity generating scalp-recorded EEG rhythms (Pascual-Marqui, 2007). The present implementation of eLORETA uses a realistic head volume conductor model consisting of the scalp, skull, and cerebral cortex. Exploring electrodes can be virtually positioned in the scalp compartment to provide EEG data as input for source estimation (Pascual-Marqui, 2007). These compartments of the head model are based on a template used in many neuroimaging studies, namely that of the Montreal Neurological Institute (i.e., the MNI152 template).

The input for the eLORETA source estimation in the present study was the artifact-free EEG epochs with 19 scalp electrodes placed according to the 10–20 montage system. The output is the set of estimates of neural ionic currents in the equivalent current dipoles located in the 6,239 voxels with 5 mm resolution, restricted to the cortical gray matter of the realistic head volume conductor model. In that cortical source space, an equivalent current dipole is located at the center of each voxel. The eLORETA package provides the Talairach coordinates, the cortical lobe, and the Brodmann area (BA) of each voxel.

The eLORETA freeware solves the so-called regularized EEG linear inverse problem, estimating "neural" current density values at any cortical voxel of the realistic head volume conductor model mentioned. The solutions are computed at each EEG frequency bin (e.g., in the present study, 0.25 Hz as frequency resolution, namely, the maximum frequency resolution allowed using 4-s artifact-free EEG epochs).

A regional analysis of the eLORETA solutions was performed in the following lobar macro-regions of interest (ROIs): frontal (Brodmann area, BA 8, 9, 10, 11, 44, 45, 46, and 47), central (BA 1, 2, 3, 4, and 6), parietal (BA 5, 7, 30, 39, 40, and 43), occipital (BA 17, 18, and 19), and temporal (BA 20, 21, 22, 37, 38, 41, and 42). Remarkably, the eLORETA solution for each of these lobar ROIs was obtained by averaging the normalized eLORETA current density values estimated at all included individual voxels. For example, the eLORETA solution for the temporal ROI was obtained by averaging the normalized eLORETA current density values estimated at all voxels included in the BA 20, 21, 22, 37, 38, 41, and 42 of the bilateral temporal lobes.

2.7. Statistical analysis

The statistical analyses of the present study were performed by the STATISTICA software, version 10.0 (StatSoft Inc., www.statsoft.com).

To test the working hypothesis of the present study, the regional eLORETA EEG source activities were compared across the different recording conditions in the t-Nold and t-ADMCI subgroups.

The statistical comparisons of the EEG source activity were performed using ANOVA models with statistical significance set at $p < 0.05$. Mauchly's test for sphericity was used to assess whether the assumption of sphericity was met, and the Greenhouse-Geisser correction was applied if the data violated that assumption. The Duncan test was used for post-hoc comparisons ($p < 0.05$, Bonferroni corrected).

Since the use of ANOVA models implies that the dependent variable must be normally distributed, the Kolmogorov-Smirnov test ($p < 0.05$) was used to determine whether the regional eLORETA EEG source activities approximated Gaussian distributions (null hypothesis of non-Gaussian distributions tested at $p < 0.05$). This prerequisite was not met in some cases, so all regional eLORETA source activities were used as inputs to the log 10 transformation to make those eLORETA solutions Gaussian. The Kolmogorov-Smirnov test confirmed that all regional eLORETA source activities were Gaussian after that transformation ($p > 0.05$). These activities were used for the statistical sessions described in the following paragraphs. For each ANOVA model, variables showing significant differences in post-hoc comparisons were examined for the presence of possible outliers using Grubbs' iterative method at $p < 0.001$. If outliers were detected, the analysis was repeated with their removal to confirm the robustness of the results.

The first statistical session tested the hypothesis of differences in the regional eLORETA EEG source activities between the t-Nold ($N = 11$) and t-ADMCI ($N = 18$) groups ($p < 0.05$). The ANOVA factors were Group (t-ADMCI and t-Nold; independent variable), Condition (Eyes

Open, Wakefulness, Flattening, and Ripples), Frequency Band (delta, theta, alpha 1, alpha 2, and alpha 3), and ROI (Frontal, Parietal, and Occipital). The confirmation of the hypothesis required a statistically significant ANOVA effect including the factors Group ($p < 0.05$) and Condition, and a post-hoc Duncan test confirming the statistically significant differences in the eLORETA source solutions between the t-Nold and t-ADMCI groups ($p < 0.05$).

The second statistical session tested the hypothesis that the regional eLORETA EEG source activities of the t-Nold ($N = 11$) and t-ADMCI ($N = 18$) groups differed during the transition from the resting-state Eyes Closed to the Eyes Open conditions ($p < 0.05$). For this purpose, the dependent variable was the ratio of the regional eLORETA rsEEG source activities between the Eyes Closed and Eyes Open conditions. The ANOVA factors were Group (t-Nold and t-ADMCI; independent variable), Frequency Band (delta, theta, alpha 1, alpha 2, and alpha 3), and ROI (Frontal, Parietal, and Occipital). The confirmation of the hypothesis required a statistically significant ANOVA effect, including the factor Group ($p < 0.05$) and a post-hoc Duncan test confirming the statistically significant differences in the eLORETA source solutions between the t-Nold and t-ADMCI groups ($p < 0.05$).

The third statistical session tested the hypothesis that the regional eLORETA EEG source activities of the t-Nold ($N = 11$) and t-ADMCI ($N = 18$) groups differed ($p < 0.05$) during the transition from the Wakefulness to Ripple stages of the Vigilance condition. For this purpose, the dependent variable was the ratio of the regional eLORETA EEG source activity between the Wakefulness and the Ripple stages. The ANOVA factors were Group (t-Nold and t-ADMCI; independent variable), Frequency Band (delta, theta, alpha 1, alpha 2, and alpha 3), and ROI (Frontal, Parietal, and Occipital). The confirmation of the hypothesis required a statistically significant ANOVA effect, including the factor Group ($p < 0.05$) and a post-hoc Duncan test confirming the statistically significant differences in the eLORETA source solutions between the t-Nold and t-ADMCI groups ($p < 0.05$).

3. Results

Supplementary Materials Figure SM2 illustrates the mean (± SE) regional eLORETA EEG source activities in the t-Nold ($N = 11$) and t-ADMCI ($N = 18$) groups for all variables of interest, such as the resting-state Eyes Open condition, the stages of the Vigilance condition (i.e., Wakefulness, Flattening, and Ripples), the frequency bands (delta, theta, alpha 1, alpha 2, and alpha 3), and the ROIs (Frontal, Central, Parietal, Temporal, and Occipital). In the t-Nold group, the regional eLORETA EEG sources showed the expected prominent activities at the alpha 2 and alpha 3 bands estimated during the Wakefulness stage, with a topographic gradient showing the maximum activities at the occipital ROI with a gradual reduction in magnitude towards the anterior regions. The mean group values of TF and IAFp were 5.9 (± 0.2) Hz and 9.6 (± 0.3) Hz in the Nold group, while they were 5.4 (± 0.2) Hz and 8.8 (± 0.3) Hz in the ADMCI group (see Table 1). Furthermore, there was the expected widespread reduction in the regional eLORETA EEG alpha 2 and alpha 3 source activities estimated during the resting-state Eyes Open condition and the Flattening and Ripples stages. Finally, there was an expected increase in the regional eLORETA EEG theta source activities during the Ripples stage. Compared to the t-Nold group, the t-ADMCI group was characterized by lower regional eLORETA rsEEG alpha 2 and alpha 3 source activities estimated during the Wakefulness stage and high regional eLORETA EEG delta and theta source activities in all phases of the recording. Overall, these features of the regional eLORETA EEG source activities indicated the acceptable quality of the experimental procedures of EEG data recording and analysis.

The results of the first statistical session (see Fig. 2) showed a statistically significant ANOVA interaction [$F(24, 648) = 1.5729$; $p = 0.040$] among the factors Group (t-ADMCI and t-Nold; independent variable), Condition (Eyes Open, Wakefulness, Flattening, and Ripples), Frequency Band (delta, theta, alpha 1, alpha 2, and alpha 3), and ROI (Frontal, Parietal, and Occipital). The planned post-hoc Duncan testing was focused on the comparison of the regional eLORETA EEG delta and alpha source activities between the two groups and unveiled the following results. Compared to the t-Nold group, the t-ADMCI group was characterized by greater frontal eLORETA EEG delta source activities at the Wakefulness ($p = 0.0023$, $p < 0.05$ uncorrected), Flattening ($p = 0.0011$, $p < 0.05$ uncorrected), and Ripples ($p = 0.0002$, $p < 0.05$ with Bonferroni correction for 4 ROI *5 frequency bands * 3 conditions = 60, $p < 0.05/60 = 0.0008$) stages of the Vigilance condition. The t-ADMCI group was also characterized by lower occipital eLORETA EEG alpha 2 and alpha 3 source activities estimated during the Vigilance stage of Wakefulness ($p = 0.0253$ and $p = 0.0211$, respectively; $p < 0.05$ uncorrected). Data distributions for both groups were examined, and Grubbs' iterative method for outlier detection with $p < 0.001$ was performed on those source activity values that showed significant differences in post hoc tests (i.e., frontal delta source activities in Wakefulness, Flattening, and Ripples, and occipital alpha 2 and alpha 3 source activities in Wakefulness). No outliers were found for t-ADMCI and t-Nold participants (see Figure SM3).

The second statistical session used the ratio of the regional eLORETA EEG source activities between the Wakefulness stage and the Eyes-Open condition as a dependent variable to probe the ***reactivity*** of EEG alpha sources during the vigilance transition from brain arousal to quiet vigilance. The results of this session showed that the ANOVA interaction among the factors Group (t-ADMCI and t-Nold; independent variable), Frequency Band (delta, theta, alpha 1, alpha 2, and alpha 3), and ROI (Frontal, Parietal, and Occipital) was not statistically significant [$F(8, 216) = 1.9553$, $p = 0.0534$], possibly due to relatively small sample size. Notably, descriptive data showed the expected reduction in the rsEEG occipital source activities in the t-ADMCI group compared to the t-Nold group (see Fig. 3).Outliers detection (Grubbs' iterative method with $p < 0.001$) identified only 3 outliers (2 t-ADMCI subjects and 1 t-Nold subject) in the values of interest (occipital alpha 2 and occipital alpha 3; see Figure SM4).

The third statistical session used the ratio of the regional eLORETA EEG source activities between the Wakefulness and Ripples stages as a dependent variable to probe the ***reactivity*** of the EEG alpha sources during the vigilance transition from quiet vigilance to light NREM sleep. The results of this session (see Fig. 4) showed a statistically significant ANOVA interaction [$F(8, 216) = 1.9936$; $p = 0.0489$] among the factors Group (t-ADMCI and t-Nold; independent variable), Frequency Band (delta, theta, alpha 1, alpha 2, and alpha 3), and ROI (Frontal, Parietal, and Occipital). The planned post-hoc Duncan testing was focused on the high-frequency alpha source activities and showed that the t-ADMCI group was characterized by lower reactivity of the eLORETA EEG alpha 2 and alpha 3 source activities estimated in the occipital (both $p < 0.0001$; $p < 0.05$ Bonferroni correction for 3 ROI *5 frequency bands = 15, $p < 0.05/15 = 0.0033$) and parietal ($p < 0.01$ and $p < 0.005$, respectively; $p < 0.05$ uncorrected) ROIs compared to the t-Nold group. Since Grubbs' iterative method ($p < 0.001$) detected 3 outliers (2 t-ADMCI and 1 t-Nold; see Figure SM5) in the values with significant differences in post-hoc tests, the ANOVA was repeated, excluding the outliers. The results confirm those obtained on the whole sample [$F(8, 192) = 3.2616$, $p = 0.0017$; all post-hoc tests p-values < 0.05 with Bonferroni correction for alpha 2 and alpha 3 source activities in parietal and occipital ROIs].

3.1. Results of the control analyses

The above results showed that the t-ADMCI group was characterized by significant differences in regional eLORETA EEG delta and alpha 2–3 source activities during the three stages of the Vigilance condition (i.e., Wakefulness, Flattening, and Ripples) compared to the t-Nold group. These results motivate future studies comparing t-ADMCI participants and those ***not*** showing the transitions of the EEG activity across the Vigilance stages (nt-ADMCI). These results also motivate future studies

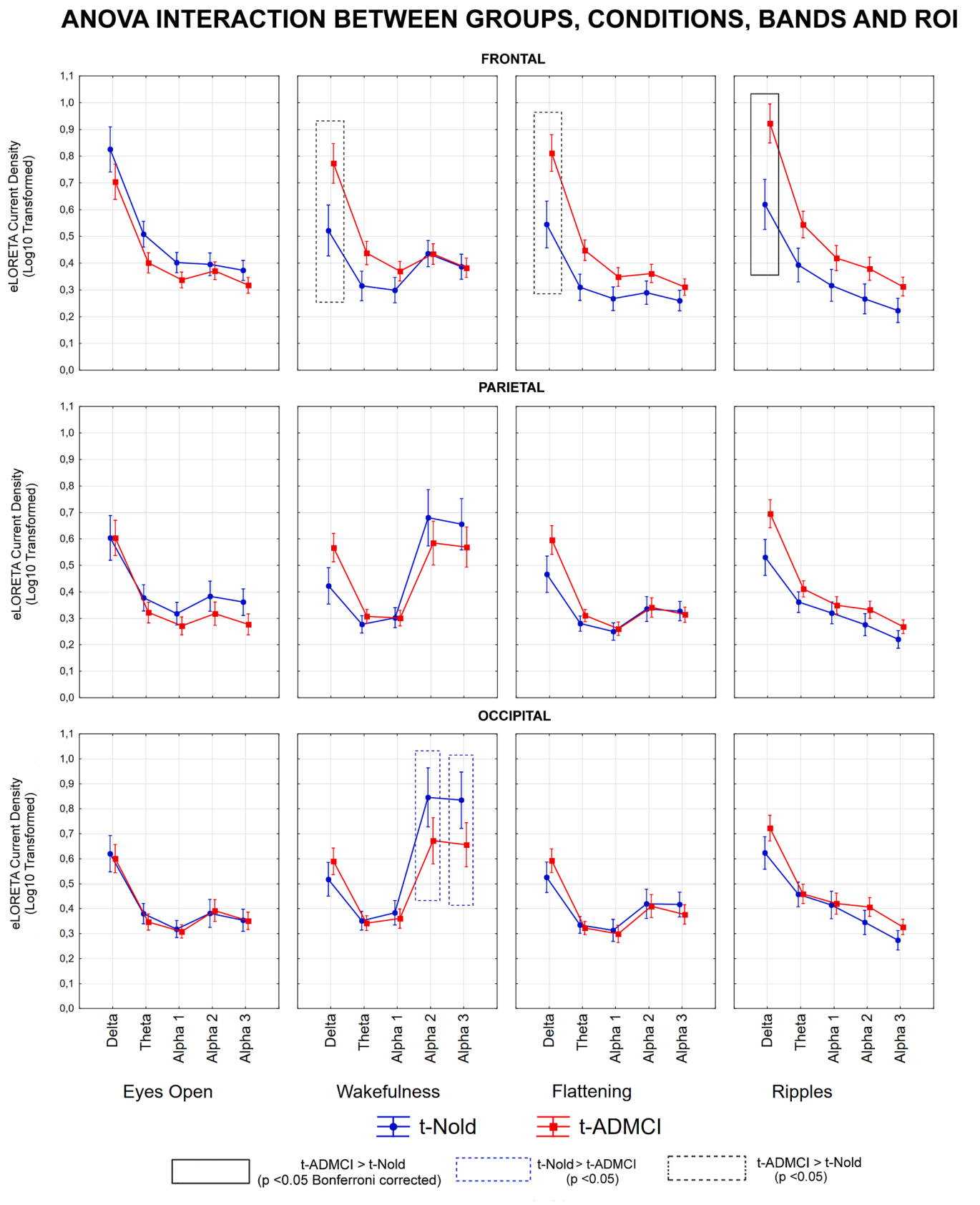

(caption on next page)

Fig. 2. Regional normalized exact low-resolution brain electromagnetic tomography (eLORETA) solutions (mean across subjects, log-10 transformed) modelling cortical sources of Vigilance electroencephalographic (EEG) rhythms relative to a statistical ANOVA interaction among the factors Group (healthy elderly subjects showing transitions to light sleep, t-Nold, N = 11; patients with mild cognitive impairment due to Alzheimer's disease showing transitions to light sleep, t-ADMCI N = 18); Frequency Band (Delta, Theta, Alpha 1, Alpha 2, Alpha 3), Region of Interest (ROI; Frontal, Parietal, Occipital), and Condition (Eyes Open, Wakefulness, Flattening, Ripples). This ANOVA design used the regional normalized eLORETA solutions as a dependent variable. Regional normalized eLORETA solutions modelled the EEG relative power spectra as revealed by a sort of "virtual" intracranial macro-electrodes located on the macro-cortical regions of interest. Legend: black rectangles indicate the cortical regions and frequency bands in which the eLORETA solutions presented a statistically significant pattern t-ADMCI > Nold after post-hoc analysis (dashed line: $p < 0.05$; filled line: $p < 0.05$ Bonferroni corrected, i.e. $p < 0.0008$), blue dashed rectangles indicate the cortical regions and frequency bands in which the eLORETA solutions presented a statistically significant pattern t-ADMCI < Nold after post-hoc analysis ($p < 0.05$). (For interpretation of the references to colour in this figure legend, the reader is referred to the web version of this article.)

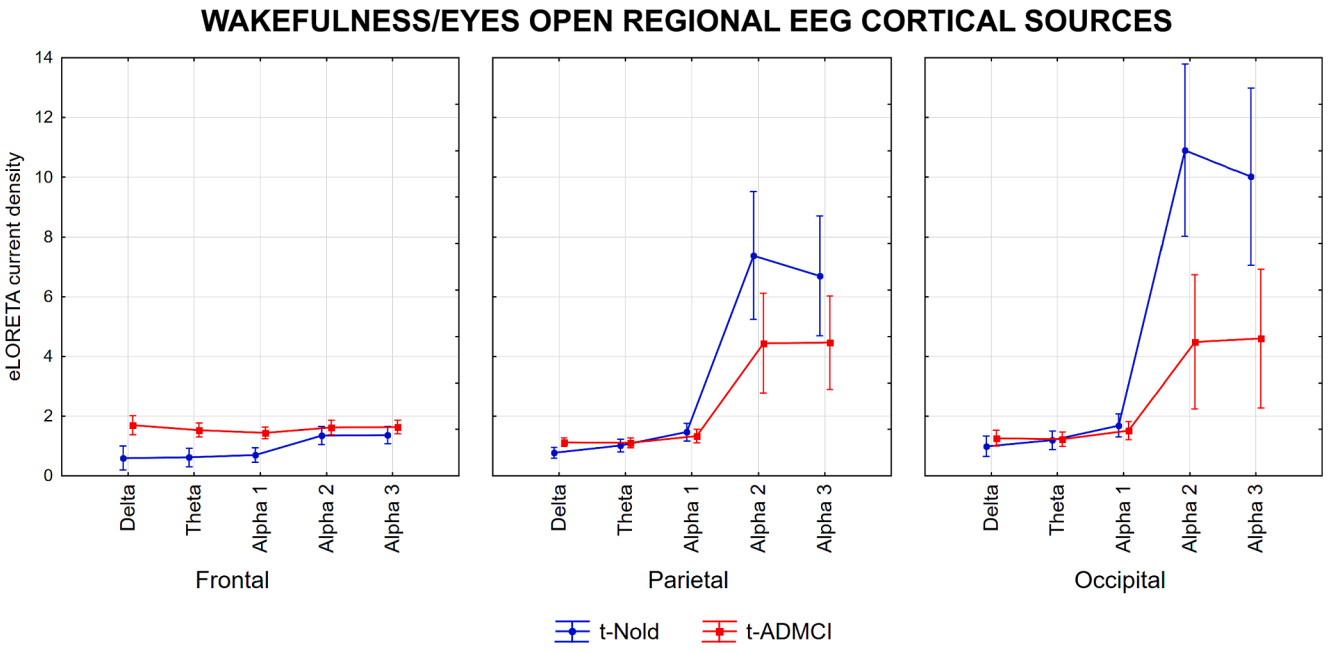

Fig. 3. Regional normalized exact low-resolution brain electromagnetic tomography (eLORETA) solutions (mean across subjects) modelling the ratio of cortical sources of the electroencephalographic (EEG) rhythms in the Wakefulness and Eyes Open conditions (Wakefulness/Eyes Open) for healthy elderly subjects showing transitions to light sleep (t-Nold, N = 11) and patients with mild cognitive impairment due to Alzheimer's disease showing transitions to light sleep (t-ADMCI N = 18) across EEG frequency bands (Delta, Theta, Alpha 1, Alpha 2, Alpha 3), and regions of interest (ROI; Frontal, Parietal and Occipital).

comparing t-Nold participants and those ***not*** showing the transitions of the EEG activity across the Vigilance stages (nt-Nold). In the following, we performed three control analyses to probe the effect size for those studies.

The first control analysis tested the effect size from the comparison between the t-ADMCI (N = 18) and nt-ADMCI (N = 16) subgroups in the regional eLORETA EEG delta and high-frequency alpha source activities during the resting-state eyes-closed condition. A control ANOVA addressed this issue ($p < 0.05$) using as a dependent variable the regional eLORETA EEG source activities estimated for the resting-state Eyes Closed condition. The ANOVA factors were Group (t-ADMCI and nt-ADMCI; independent variable), Frequency Band (delta, theta, alpha 1, alpha 2, and alpha 3), and ROI (Frontal, Parietal, and Occipital). The results showed an ANOVA interaction among group, frequency band, and ROI [$F(8, 256) = 2.2731$, $p = 0.0230$] (see Fig. 5). Planned post-hoc Duncan testing ($p < 0.05$ with Bonferroni correction for 5 frequency bands, $p < 0.05/5 = 0.01$) revealed that the t-ADMCI group was characterized by greater eLORETA EEG delta source activities in frontal ($p = 0.0099$; $p < 0.05$ uncorrected), parietal ($p = 0.0001$; $p < 0.05$ corrected), and occipital ($p = 0.0001$; $p < 0.05$ corrected) regions compared to the nt-ADMCI group, as well as higher occipital theta source activity ($p = 0.0407$; $p < 0.05$ uncorrected). Data distributions for t-ADMCI and nt-ADMCI are shown in Figure SM6. Grubbs' iterative method with $p < 0.001$ found no outliers in source activity values showing significant differences according to post hoc tests. The data on the basis of these statistical effects were used as an input to compute effect sizes by Cohen's d (Cohen, 1988) and the sample size by an alpha level of 0.05 and a desired power of 0.8. The following Cohen's d values (and corresponding sample size for each group) were produced for the occipital (d = 1.54, suggested sample size: 7 subjects), parietal (d = 1.31, suggested sample size: 10 subjects), and global (d = 1.31, suggested sample size: 14 subjects) EEG delta sources.

Notably, these results were not attributable to significant differences between the nt-ADMCI and t-ADMCI groups based on relevant demographic and genetic data, clinical information and biomarkers (i.e., CSF amyloid and tau, MRI), and neuropsychological test scores, as shown in Table 4 (see above) and the tables described below. Table 5 reports the mean scores (± SE) of the neuropsychological tests assessing cognitive functions in the two ADMCI groups. These tests included the Alzheimer's Disease Assessment Scale-Cognitive Subscale (ADAS-Cog), the Immediate and Delayed Recall Logical Memory Test, the Immediate and Delayed Recall Rey Auditory Verbal Memory Test, the Clock Drawing Test, The Trail Making Test B-A, the Verbal Fluency for Letters and Verbal Fluency for Categories. No statistically significant difference in those variables was found between the two groups ($p > 0.05$). In particular, language abilities typically reflect crystallized intelligence. Along the same line, the two ADMCI subgroups did not differ in other typical dementia risk factors, such as living alone (yes/no), socioeconomic status (coded in low, middle, and high based solely on the subjects' job occupations), and familiarity history of dementia (yes if at least one of mother, father, or siblings has been diagnosed with dementia). Results showed no statistical effects between the two subgroups

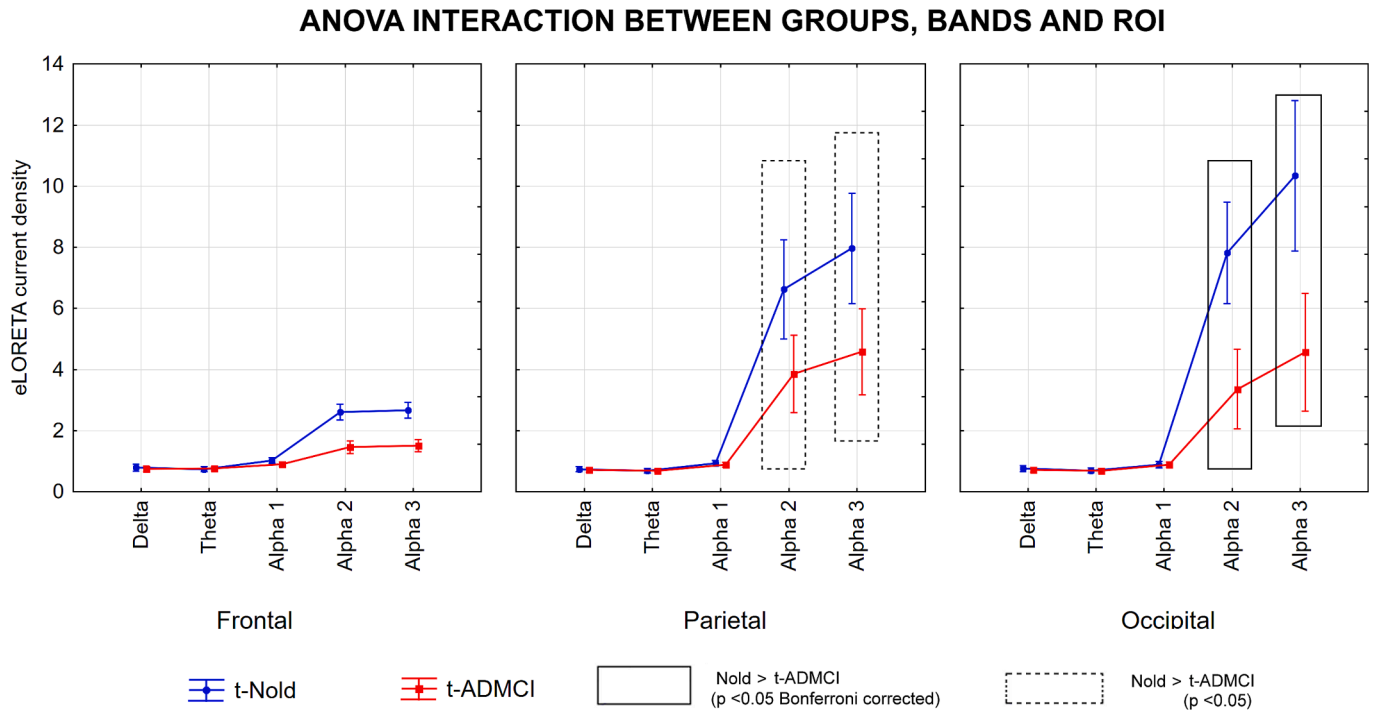

Fig. 4. Regional normalized exact low-resolution brain electromagnetic tomography (eLORETA) solutions (mean across subjects, log-10 transformed) modelling the ratio of cortical sources of the electroencephalographic (EEG) rhythms in the Wakefulness and Ripples conditions (Wakefulness/Ripples) and relative to a statistical ANOVA interaction among the factors Group (healthy elderly subjects showing transitions to light sleep, t-Nold, N = 11; patients with mild cognitive impairment due to Alzheimer's disease showing transitions to light sleep, t-ADMCI N = 18), Frequency Band (Delta, Theta, Alpha 1, Alpha 2, Alpha 3), and Region of Interest (ROI; Frontal, Parietal and Occipital). Legend: the rectangles indicate the cortical regions and frequency bands in which after a post-hoc analysis using Duncans's method the eLORETA solutions presented a statistically significant eLORETA pattern t-ADMCI > Nold (dashed line $p < 0.05$; filled line: $p < 0.05$ Bonferroni corrected, i.e. $p < 0.003$).

($p > 0.05$; Table 5). The lack of statistical effects in the present relatively small ADMCI samples (t-ADMCI, N = 18; nt-ADMCI, N = 16) provides a first hint that core results may not be strongly affected by premorbid intelligence and the above confounding variables.

Table SM2 reports mean values (± SE) of the T1-weighted and T2-weighted FLAIR MRI biomarkers probing brain gray matter volumes and thickness and white matter hypointensity and lesions in the two ADMCI groups. The variables of interest included the volumes of the ventricles, hippocampus, amygdala, thalamus, and basal ganglia nuclei. They also included the thickness of several cortical regions. No statistically significant difference in those variables was found between the two groups ($p > 0.05$). Furthermore, the two subgroups differed neither in the MRI-FLAIR markers of subcortical white matter lesions ($p > 0.05$ uncorrected) typically reflecting cardiovascular risk factors nor in the clinical indexes of cardiovascular risk factors such as body mass index, systolic blood pressure, diastolic blood pressure, and heart rate ($p > 0.05$).

Table SM3 reports the mean values (± SE) of the diffusion MRI biomarkers (i.e., fractional anisotropy and diffusivity) probing several brain white matter tracts in the two ADMCI groups. No statistically significant difference in those variables was found between the two groups ($p > 0.05$).

The second control analysis tested the effect size from the comparison between the t-Nold (N = 11) and nt-Nold (N = 11) subgroups in the regional eLORETA EEG delta and high-frequency alpha source activities during the resting-state eyes-closed condition. The ANOVA dependent variable was the regional eLORETA EEG source activities estimated for the resting-state Eyes Closed condition. The ANOVA factors were Group (t-Nold and nt-Nold; independent variable), Frequency Band (delta, theta, alpha 1, alpha 2, and alpha 3), and ROI (Frontal, Parietal, and Occipital). Notably, there were no differences in age, education, and MMSE scores between the two groups ($p > 0.05$). The results (see Fig. 6) showed an interaction between the factors Group and Frequency Band [$F(4, 80) = 4.4920$, $p = 0.0025$]. Planned post-hoc Duncan tests focused on comparisons between the two groups. They showed that the t-Nold group was characterized by lower global eLORETA EEG alpha 2 and alpha 3 source activities compared to the nt-Nold group ($p = 0.0285$ and $p = 0.0313$, respectively, $p < 0.05$ uncorrected). ($p < 0.05$ uncorrected). Fig. 6 illustrates these results. No outliers were detected in the source activities that showed significant differences in post-hoc tests (Grubb's iterative method with $p < 0.001$; data distributions for t-Nold and nt-Nold groups are shown in Figure SM7). The data on the basis of these statistical effects were used as an input to compute effect sizes by Cohen's d and the sample size by an alpha level of 0.05 and a desired power of 0.8. The following Cohen's d values (and corresponding suggested sample size) were produced: 0.69 (33 subjects) for the global rsEEG alpha 2 source activity and 0.77 (27 subjects) for the global rsEEG alpha 3 source activity.

The main study results also raised two questions. The first question was whether the regional eLORETA EEG source activities in ADMCI patients might be characterized by the high variability of those activities over EEG recordings lasting only a few minutes (i.e., 3–5 min). Two control ANOVAs addressed this question ($p < 0.05$), one for the t-ADMCI group and the other for the nt-ADMCI group. For each ANOVA, the dependent variable was the regional eLORETA EEG source activities estimated during the resting-state Eyes Closed condition. At the end of the preliminary EEG data analysis, each ADMCI patient was associated with artifact-free EEG epochs of 4 s recorded during that condition. They were divided into two classes: the EEG epochs recorded during the first half of the resting-state Eyes Closed condition (i.e., 1.5–2.5 min) and those recorded during the second half. For each ADMCI group (t-ADMCI or nt-ADMCI), the ANOVA factors were Condition (First half and Second half; independent variable), Frequency Band (delta, theta, alpha 1, alpha 2, and alpha 3), and ROI (Frontal, Parietal, and Occipital). The results

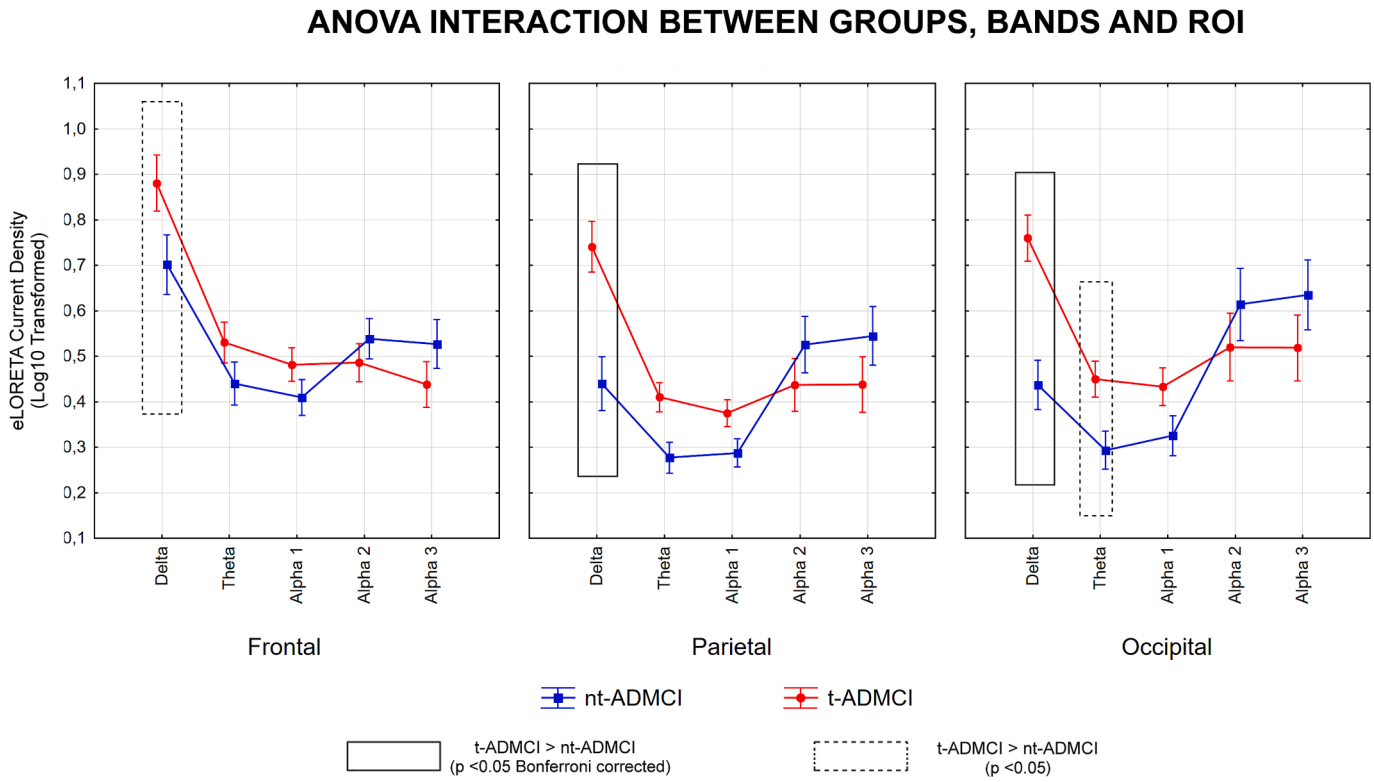

Fig. 5. Regional normalized exact low-resolution brain electromagnetic tomography (eLORETA) solutions (mean across subjects, log-10 transformed) modelling cortical sources of the resting state electroencephalographic (rsEEG) rhythms in patients with mild cognitive impairment due to Alzheimer's without transitions to light sleep (nt-ADMCI, N = 16) and patients with mild cognitive impairment due to Alzheimer's disease showing transitions to light sleep (t-ADMCI, N = 18). Results of the statistical ANOVA interaction among the factors Group (nt-ADMCI vs. t-ADMCI), Frequency Band (Delta, Theta, Alpha 1, Alpha 2, Alpha 3), and Region of Interest (ROI; Frontal, Parietal, Occipital) are presented. Legend: the rectangles indicate the cortical regions and frequency bands in which after a post-hoc analysis using Duncans's method the eLORETA solutions presented a statistically significant pattern t-ADMCI > nt-ADMCI (dashed line: $p < 0.05$; filled line: $p < 0.05$ Bonferroni corrected, i.e., $p < 0.003$).

Table 5
Neuropsychological data and results of their statistical comparisons ($p < 0.05$) in t-ADMCI and nt-ADMCI participants. *Legend:* t-ADMCI: participants with mild cognitive impairment due to Alzheimer's disease transitioning into light sleep; nt-ADMCI: participants with mild cognitive impairment due to Alzheimer's disease not transitioning into light sleep; ADAS-Cog: Alzheimer's disease assessment scale – Cognition; n.s. = not significant ($p > 0.05$).

Neuropsychological tests scores in t-ADMCI and nt-ADMCI participants (mean ± SE)				
	t-ADMCI (N = 16) [a]	**nt-ADMCI (N = 16)**	**T-test**	**Cut-off**
ADAS-Cog	19.7 ± 2.5 (66.7 %)	22.3 ± 1.8 (75 %)	n.s.	> 17
Logical memory, immediate recall	8.3 ± 1.6 (81.3 %)	7.2 ± 4.8 (87.5 %)	n.s.	< 13
Logical memory, delayed recall	7.3 ± 1.6 (75.0 %)	5.1 ± 0.9 (100 %)	n.s.	< 12
Auditory verbal memory test, immediate recall	33.7 ± 3.0 (37.5 %)	31.3 ± 2.5 (31.3 %)	n.s.	< 28.53
Auditory verbal memory test, delayed recall	4.1 ± 0.9 (56.3 %)	3.9 ± 0.8 (68.8 %)	n.s.	< 4.96
Clock drawing test	3.8 ± 0.4 (81.3 %)	4.2 ± 0.2 (87.5 %)	n.s.	> 3
Trail making test B-A	129.6 ± 17.5 (23.5 %)	151.4 ± 19.1 (18.8 %)	n.s.	> 186
Verbal fluency for letters	31.0 ± 2.0 (0.0 %)	36.3 ± 2.3 (0.0 %)	n.s.	< 17
Verbal fluency for categories	33.9 ± 3.1 (37.5 %)	31.7 ± 3.1 (12.5 %)	n.s.	< 25

[a] : neuropsychological data were not available for 2 t-ADMCI participants in the original group of 18 t-ADMCI subjects.

showed statistically significant effects neither for the t-ADMCI group ($p > 0.05$) nor for the nt-ADMCI group ($p > 0.05$), suggesting that the changes in the regional eLORETA EEG source activities during the Vigilance condition were not due to an intrinsic unreliability of the variable. For a relatively short period of the resting-state Eyes Closed condition (i.e., 3–5 min), the regional eLORETA EEG source activities were stable in both the t-ADMCI and nt-ADMCI groups. For illustrative purposes, Figure SM8 illustrates the mean regional eLORETA source activities in the t-ADMCI and nt-ADMIC groups for the mentioned bands and ROIs during the two halves of the resting-state Eyes Closed condition.

The second question was whether the use of a relatively low number of scalp electrodes to record EEG data may have induced poor eLORETA source estimations, affecting the reactivity of EEG alpha source activities from the Wakefulness to the Ripple's stages (i.e., one of the core results). A control ANOVA using EEG power density computed across all scalp electrodes (i.e., the global EEG power density) addressed this question at the low spatial resolution of EEG spectral solutions obtained at the scalp sensors ($p < 0.05$). The ANOVA dependent variable was the ratio of the global EEG power density between Wakefulness and Ripple's stages. The ANOVA factors were Group (t-ADMCI and t-Nold; independent variable) and Frequency Band (delta, theta, alpha 1, alpha 2, and alpha 3). The results showed a statistically significant ANOVA interaction [$F(4, 88) = 3{,}8888$; $p = 0.00590$] between the factors (**see** Fig. 7). The planned post-hoc Duncan testing showed that the t-ADMCI group was characterized by lower reactivity of the global alpha 3 power density ratio ($p < 0.001$). The results globally confirmed at the scalp level those obtained on EEG source space.

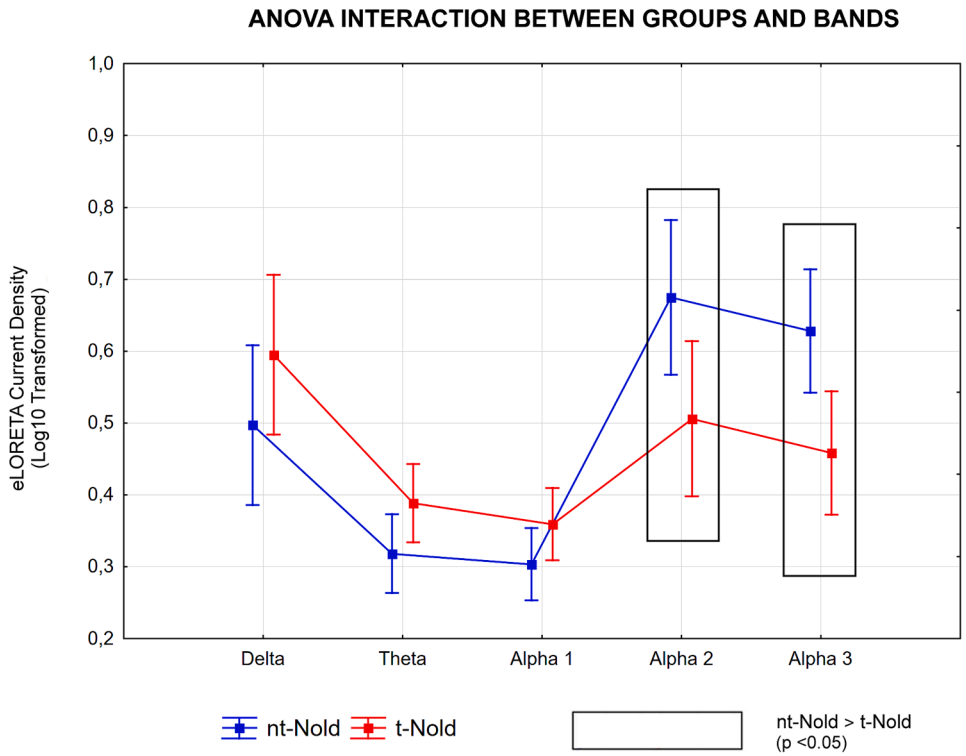

Fig. 6. Regional normalized exact low-resolution brain electromagnetic tomography (eLORETA) solutions (mean across subjects, log-10 transformed) modelling cortical sources of the resting state electroencephalographic (rsEEG) rhythms in healthy elderly subjects not showing transitions to light sleep (nt-Nold, N = 11) and healthy elderly subjects showing transitions to light sleep (t-Nold, N = 11). Results of the statistical ANOVA interaction among the factors Group (nt-Nold vs. t-Nold), Frequency Band (Delta, Theta, Alpha 1, Alpha 2, Alpha 3) are presented. Legend: the rectangles indicate the cortical regions and frequency bands in which after a post-hoc analysis using Duncans's method the eLORETA solutions presented a statistically significant pattern nt-Nold > t-Nold ($p < 0.05$).

4. Discussion

In this exploratory study of clinical neurophysiology, we investigated for the first time whether ongoing EEG activity collected during a daytime recording session may exhibit abnormalities in ADMCI patients, specifically during the transition from quiet wakefulness to light NREM sleep. This transition was examined as a potential neurophysiological substrate of the vigilance dysfunctions observed in ADMCI (Bonanni et al., 2005; Brzecka et al., 2018; Fang et al., 2023; Peter-Derex et al., 2015). A methodological innovation of our study was the use of a 30-minute EEG recording protocol designed to capture the transition from the resting-state, eyes-closed wakefulness stage—dominated by posterior rsEEG alpha rhythms—to the light NREM stage of Ripples, which is characterized by widespread rsEEG theta rhythms.

Visual analysis of EEG activity allowed us to classify each participant based on whether they displayed (t) or did not display (nt) the transition of EEG rhythms from Wakefulness to Ripples. Our findings are as follows: approximately 50 % of both Nold and ADMCI participants exhibited this transition (t). In comparing the t-Nold control group with the t-ADMCI group, we observed that the t-ADMCI group exhibited increased frontal EEG delta rhythms across the Wakefulness, Flattening, and Ripples stages. Additionally, the t-ADMCI group showed reduced reactivity in posterior EEG alpha rhythms from the Wakefulness to Ripples stages.

These findings suggest that the abnormalities in EEG rhythms observed in ADMCI patients, particularly during the transition from wakefulness to light NREM sleep, may reflect underlying vigilance dysfunctions in this population.

4.1. Thalamocortical dysrhythmia and subcortical ascending neuromodulatory systems may affect the vigilance transition to diurnal sleep in ADMCI patients

The widespread EEG delta rhythms and reduced reactivity of posterior EEG alpha rhythms observed in t-ADMCI patients during the transition to light sleep suggest a potential thalamocortical dysrhythmia at frequencies below 7 Hz, possibly contributing to the dysregulation of quiet vigilance (Jeanmonod et al., 1996; Llinás and Steriade, 2006). According to the thalamocortical dysrhythmia theory, neurological patients with cognitive and motor deficits often exhibit dominant resting-state EEG delta-theta rhythms rather than alpha rhythms due to a slowing of cortical pyramidal neuron activity to frequencies below 7 Hz. This slowing is thought to arise from the "bursting mode" of thalamocortical and corticothalamic circuit neurons, which is triggered by reduced excitatory input (Jeanmonod et al., 1996; Llinás and Steriade, 2006). In this "bursting mode," thalamocortical neurons experience prolonged membrane hyperpolarization between action potential bursts, limiting their capacity to relay excitatory inputs effectively and thereby impairing cortical arousal and vigilance regulation (Jeanmonod et al., 1996; Llinás and Steriade, 2006).

Prior MRI studies have shown significant structural abnormalities in thalamocortical and corticothalamic circuits in AD patients, which may provide insights into the neural basis for these dysrhythmic patterns. Diffusion tensor imaging (DTI) studies, for instance, have demonstrated microstructural white-matter abnormalities extending from thalamic radiations to the cerebral cortex in ADD patients compared to healthy controls (Bergamino et al., 2021; Kuhn et al., 2021; Mayo et al., 2017; Singh et al., 2024; Xiao et al., 2022; Zhong et al., 2023; Zhu et al., 2015). These microstructural abnormalities in thalamic radiation have also been correlated with fluid biomarkers of AD-related neuropathology and

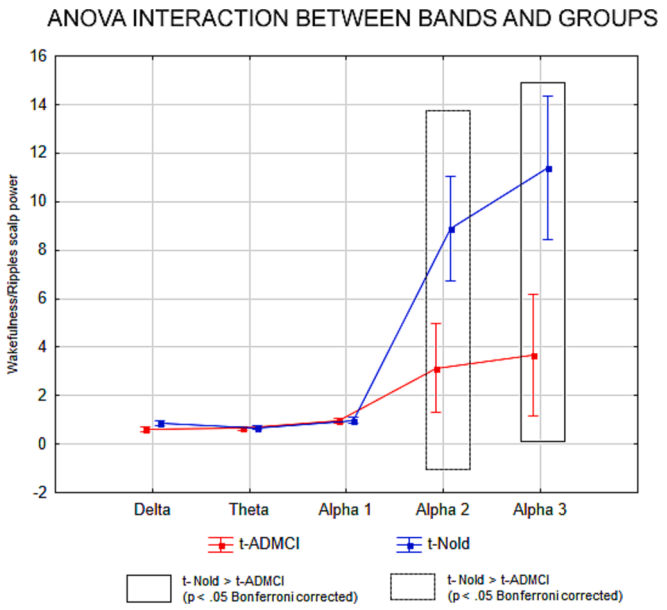

Fig. 7. Normalized global spectral power densities (computed across all scalp electrodes) modelling the ratio of the electroencephalographic (EEG) rhythms in the Wakefulness and Ripples conditions (Wakefulness/Ripples) and relative to a statistical ANOVA interaction among the factors Group (healthy elderly subjects showing transitions to light sleep, t-Nold, N = 11; patients with mild cognitive impairment due to Alzheimer's disease showing transitions to light sleep, t-ADMCI N = 18) and Frequency Band (Delta, Theta, Alpha 1, Alpha 2, Alpha 3). Legend: the rectangles indicate the cortical regions and frequency bands in which after a post-hoc analysis using Duncans's method the eLORETA solutions presented a statistically significant eLORETA pattern t-ADMCI > Nold (dashed line $p < 0.05$; filled line: $p < 0.05$ Bonferroni corrected, i.e. $p < 0.003$).

vigilance dysfunctions, such as apathy, in ADMCI patients (Nabizadeh et al., 2022; Setiadi et al., 2021; Wen et al., 2019). Moreover, volumetric MRI studies in ADMCI and ADD patients have revealed significant atrophy within thalamic nuclei, including the mediodorsal, pulvinar, and centromedial regions (Bernstein et al., 2021; van de Mortel et al., 2021). Functional MRI studies further indicate functional dysconnectivity between the thalamus and limbic and default mode networks in ADD (Qiu et al., 2022; Wu et al., 2022; Zhao et al., 2019) and ADMCI (Brueggen et al., 2016; Gilligan et al., 2019; Tang et al., 2021; Velioglu et al., 2023; Wang et al., 2022; Yu et al., 2019) patients compared to healthy controls during states of quiet vigilance.

Building on these findings, we speculate that thalamocortical dysrhythmia in ADMCI patients may stem from reduced excitatory input to both unspecific and specific thalamocortical neurons, which in turn facilitates slow-frequency oscillatory activity. This reduced excitatory input may be linked to dysfunction in subcortical activating systems, including cholinergic, noradrenergic, and histaminergic pathways, which play essential roles in brain arousal regulation (Ehrenberg et al., 2023). PET studies have previously identified abnormal cholinergic tracts and nicotinic receptor binding in ADMCI patients (Nakaizumi et al., 2018; Richter et al., 2019; Sabri et al., 2018; Sultzer et al., 2022; Xia et al., 2022). Additionally, in-vivo and post-mortem analyses have documented significant abnormalities in noradrenergic systems in ADD patients (Lancini et al., 2023; Oh et al., 2022, 2019; Prokopiou et al., 2023). Post-mortem studies have also shown sex-dependent alterations in histaminergic receptors in cortical neurons (Shan et al., 2012), along with the loss of orexinergic neurons in the lateral hypothalamus and histaminergic neurons in the hypothalamic tuberomammillary nucleus, which are associated with increased homeostatic sleep drive (Oh et al., 2022, 2019).

In summary, the impairments in these subcortical ascending systems, alongside their role in modulating vigilance and attention, may contribute to the vigilance dysfunctions observed in ADMCI patients, impacting the salience network and related emotional processing circuits (Jaworska et al., 2012; Oken et al., 2006).

4.2. Methodological remarks and discussion

The present study explored changes in ongoing EEG activity during transitions from quiet wakefulness to light sleep (ripples stage) in ADMCI patients. While the present preliminary findings are promising, certain methodological considerations must be addressed to contextualize and interpret them appropriately.

The enrolled ADMCI participants were well-characterized through clinical, neuropsychological, CSF, EEG, and MRI data. However, the small size of the t-ADMCI (N = 18) and nt-ADMCI (N = 16) subgroups and the small number of participants within each clinical unit allowed neither for stratification based on time since diagnosis or pharmacological treatment neither accounting for the local equipment and procedures in the statistical models computed (see Table SM4 for details about the number of participants and EEG equipment in each clinical unit). Additionally, this small sample size, along with inherent variability from the multi-center data collection, may account for the lack of significant differences between the t-ADMCI and nt-ADMCI subgroups in the control analyses discussed in the following. Furthermore, we included relatively young (average age ~ 70) and highly educated ADMCI participants (education > 8 years) with relatively preserved global cognitive status (MMSE score of 26).

The statistical models employed in this study could only partially control for potential confounding factors, such as premorbid intelligence, cardiovascular and metabolic risk, socioeconomic status, and relevant lifestyle variables. Control analyses indicated no significant differences between the t-ADMCI and nt-ADMCI subgroups in verbal fluency scores. These serve as proxies for crystallized and premorbid verbal intelligence. Similarly, no differences were observed in the available cardiovascular and metabolic risk markers (e.g., BMI, systolic and diastolic blood pressure, and heart rate) or MRI-FLAIR indicators of subcortical white-matter lesions. Other dementia risk factors, such as living alone, socioeconomic status (based on occupational categories), and family history of dementia, also showed no significant subgroup differences in the ADMCI participants. These findings should be considered as a first indication that those variables may not have strong linear effects on the core results of the present study.

Since the accuracy of EEG source estimation depends on biological and instrumental artifacts, a rigorous protocol was employed to detect and remove them. Along this line, EEG epochs with gross movement artifacts were excluded following a visual inspection by consortium experts. ICA was applied to remove additional artifacts, with post-ICA inspections verifying the data's artifact-free status. These procedures adhere to clinical qEEG standards endorsed by the International Federation of Clinical Neurophysiology (Babiloni et al., 2020a).

A study limitation is the low spatial resolution of the present EEG techniques. EEG data were recorded from 19 scalp electrodes (10–20 International System) and post-processed using eLORETA, a source estimation technique designed to map distributed brain activity. Fine-grained spatial analyses would typically require higher electrode densities with at least 32–48 electrodes (Liu et al., 2018; Marino et al., 2016). For this reason, we ensured the robustness of the present study findings in the ADMCI participants examining the spectral characteristics of EEG activity from Wakefulness to Ripple's stages also at the scalp electrode level. The control analysis corroborated the primary findings of the EEG source-based analysis, supporting the validity of the present study's core results.

For the present exploratory study, we adapted the EEG methodological approach to the limited electrode montage available (i.e., 19 scalp electrodes of the 10–20 system) for the EEG source estimation. We used an EEG source estimation technique intrinsically designed to map distributed source activity, namely eLORETA (Pascual-Marqui, 2007).

Furthermore, EEG source estimation was focused on five broad cortical regions suitable to investigate low spatial frequency components of ongoing EEG rhythms, which can be adequately sampled with the 10–20 system. These components received extensive research looking for "microstates" in ongoing EEG activity (Khanna et al., 2015; Lehmann et al., 1987; Michel and Koenig, 2018). These "microstates" are quasi-stable topographical voltage patterns characterized by two large centroids of positive and negative potential shifting on the scalp. They are generated by widely distributed cortical networks as revealed by fMRI and can be investigated using a 10–20 montage system (Khanna et al., 2015; Michel and Koenig, 2018). Based on these considerations and data, the International Federation of Clinical Neurophysiology has endorsed the use of EEG source estimation from rsEEG data obtained with this montage in exploratory studies on neurological and psychiatric patient databases (Babiloni et al., 2020a).

The present EEG methodological approach has been previously validated in ADMCI and ADD patients by our research network (Babiloni et al., 2021b, 2020b; Rossini et al., 2020). These studies demonstrated substantial correlations between regional EEG source solutions and structural MRI gray matter volume (Babiloni et al., 2015, 2013), FDG-PET cortical hypometabolism (Babiloni et al., 2016), and resting-state fMRI connectivity (Jovicich et al., 2019) in ADMCI and ADD patients. Nevertheless, future studies should validate the current findings with a higher electrode density (32–48 scalp electrodes) and multiple EEG source estimation methods, as any source estimation inherently depends on a priori assumptions (Michel and Brunet, 2019). Furthermore, additional research should assess the reliability of regional rsEEG inverse solutions derived from 32 to 48 scalp electrodes in comparison to those obtained with 19 scalp electrodes to clarify spatial sampling dependencies of rsEEG source solutions in ADMCI patients.

Along this line, we recommend the following extension of the experimental design with the following advancements: (1) actigraphy to assess patients rest-activity rhythms and sleep-wake patterns; (2) rsEEG recordings during daytime using at least 32–48 scalp electrodes to improve EEG source estimation (3) polysomnographic recordings over two nights to better evaluate sleep architecture; (4) the application of machine learning tools to classify EEG epochs into Wakefulness, Flattening, and Ripples stages, which could have added objectivity to the classification despite the acceptable inter-rater variability (~70 %) observed in control analysis; (5) MRI analysis of the ascending subcortical neuromodulatory systems (cholinergic, dopaminergic, noradrenergic, histaminergic), which may help elucidate their role in modulating thalamocortical and corticothalamic circuits involved in arousal and vigilance-to-light sleep transitions; and (6) a 1-year follow-up to explore how disease progression affects EEG transitions from wakefulness to light sleep during daytime recordings and to assess potential associations with structural and microstructural sleep abnormalities.

5. Conclusions

This exploratory study is the first to evaluate the hypothesis that ADMCI patients may exhibit abnormal EEG rhythms during the transition from quiet wakefulness to light sleep in daytime EEG recordings, potentially reflecting vigilance dysfunctions. Results indicate that t-ADMCI patients showed increased frontal EEG delta source activities across wakefulness to Hori's Ripples stages compared to t-Nold participants. Additionally, t-ADMCI patients demonstrated a lesser reduction (reactivity) in posterior EEG alpha source activities from quiet wakefulness to Ripples. They also showed greater EEG delta source activities during quiet wakefulness than the nt-ADMCI group.

These preliminary findings support the need for a cross-validation study with a prospective, longitudinal design incorporating high-resolution EEG techniques. Future research should test the hypothesis that ADMCI patients may be more susceptible to daytime sleepiness, as identified through 24-hour actigraphy, and may exhibit distinct ongoing EEG delta and alpha rhythms during the transition from quiet vigilance to daytime naps. Validation of this hypothesis could establish EEG delta and alpha rhythms as pathophysiological "P" biomarkers indicative of vigilance dysfunctions, contributing a new biomarker dimension within the revised ATN Framework (Jack et al., 2024). Such advancements may shed light on the underexplored "dark side" of Precision Medicine in AD (Babiloni, 2022).

Disclosure statement

Financial Disclosure: none. Non-financial Disclosure: None.

Consent to participate and publication

Informed consent was obtained from all participants.

Authors' contribution

CB and EMS designed the study. CDP, GN, EMS, MC, and SL preprocessed and analyzed the EEG data. EMS, DJ, and MC performed the epoch classification. EMS, DJ, and GN performed the eLORETA analysis. EMS, CDP, and MC performed the statistical analysis. CB supervised the data analysis. EMS, MC, and RL drafted the manuscript. CB proofread and edited the manuscript. All other authors collected the data and participated in the manuscript editing and the discussion of the results.

Declaration of Competing Interest

The authors declare that they have no known competing financial interests or personal relationships that could have appeared to influence the work reported in this paper.

Acknowledgments

The present study was developed based on the data of The PDWAVES Consortium (www.pdwaves.eu) and the PharmaCog project. The electroencephalographic data recording and analysis were partially supported by the funds of "Ricerca Corrente" attributed by the Italian Ministry of Health to the IRCCS Synlab SDN of Naples (Italy), Oasi Research Institute-IRCCS, Troina (Italy), IRCCS Istituto Centro San Giovanni di Dio Fatebenefratelli (Italy), IRCCS Ospedale Policlinico San Martino, Genova (Italy), and IRCCS San Raffaele of Rome (Italy).

The Sapienza University of Rome Unit's and Ph.D. fellow Matteo Carpi's research activities were supported by the grant with the following reference: Progetto ECS 0000024 Rome Technopole, CUP B83C22002820006, PNRR Mission 4 Component 2 Investment 1.5, which was granted by European Union-NextGenerationEU.

The grant with the following reference supported Enrico Michele Salamone's Ph.D. fellowship: Azione IV.5 – on Theme "Green," D.M. August 10, 2021, n. 1061.

Claudio Babiloni was supported by the grant with the following reference: PE00000006 "PNRR MUR - M4C2 - MNESYS – A multiscale integrated approach to the study of the nervous system in health and disease (MNESYS)" - EXTENDED PARTNERSHIP #12, SPOKE 6, CASCADE CALL from PNRR, Mission 4, Component 2, Investment Grant Agreement: D33C22001340002, and eBRAIN-Health – Actionable Multilevel Health Data, Call and Sponsor: HORIZON 2021, HORIZON-INFRA-2021-TECH-01 (HORIZON-INFRA-2021-TECH-01-01 - Interdisciplinary digital twins for modeling and simulating complex phenomena at the service of research infrastructure communities), Grant Agreement: GAP-101058516.

Claudio Del Percio was partially supported by the funds of the project "Amyloid-related cortical excitability in patients with MCI due to Alzheimer's disease", Call and Sponsor: ANNUAL STRATEGIC PROGRAM OF ITALIAN MINISTRY OF UNIVERSITY AND SCIENTIFIC AND TECHNOLOGICAL RESEARCH, Grant Agreement: 2022FJAXY8.

Roberta Lizio was supported by the funds of the project titled "Fast screening of cognitive and motor functions in elderly patients with cognitive-motor deficits using digital indices: a green telemedicine service to reduce the environmental impact of mobility related to the periodic assessment of cognitive functions in healthcare facilities" from the Call PON "Green-digital" resources for technological innovation and

environmental sustainability (DM 1062/2021) Program of the Italian Ministry of University and Research.

BurcuBölükbaş was supported by the funds of the grant HORIZON 2021, H2021-MSCA-DN-2021 (Marie Skłodowska-Curie Doctoral Networks), proposal number: 101071485, title of the project: "Peripheral Biomarker-Based Combinatorial Early Diagnostics for Dementia (CombiDiag)".

John Paul Taylor is supported by the Newcastle NIHR Biomedical Research Centre.

Paolo Barone was partially supported by the funds of the project "Effects of endogenous and exogenous risk factors in patients with Alzheimer's and Parkinson's diseases using clinical indexes and endophenotypes (biomarkers) as inputs to artificial intelligence" (PREDICT-NEURODEGEN), Call and Sponsor: ANNUAL STRATEGIC PROGRAM OF ITALIAN MINISTRY OF HEALTH, Grant Agreement: PNRR-MAD-2022-12376415.

Laura Bonanni was partially supported by the funds of the project "Assessment of brain functions in Lewy Body disease patients using telemonitoring DIGITAL markers as inputs to artificial intelligence (LBDigital)", Call and Sponsor: ANNUAL STRATEGIC PROGRAM OF ITALIAN MINISTRY OF UNIVERSITY AND SCIENTIFIC AND TECHNOLOGICAL RESEARCH, Grant Agreement: 2010SH7H3F.

Appendix A. Supplementary material

Supplementary data to this article can be found online at https://doi.org/10.1016/j.clinph.2025.01.012.

References

Albert, M.S., DeKosky, S.T., Dickson, D., Dubois, B., Feldman, H.H., Fox, N.C., et al., 2011. The diagnosis of mild cognitive impairment due to Alzheimer's disease: recommendations from the National Institute on Aging-Alzheimer's Association workgroups on diagnostic guidelines for Alzheimer's disease. Alzheimers Dement J Alzheimers Assoc 7, 270–279. https://doi.org/10.1016/j.jalz.2011.03.008.

American Psychiatric Association, 2013. Diagnostic and statistical manual of mental disorders. 5th ed. Arlington, VA: Author; 2013.

Babiloni, C., 2022. The dark side of Alzheimer's disease: neglected physiological biomarkers of brain hyperexcitability and abnormal consciousness level. J Alzheimers Dis JAD 88, 801–807. https://doi.org/10.3233/JAD-220582.

Babiloni, C., Barry, R.J., Başar, E., Blinowska, K.J., Cichocki, A., Drinkenburg, W.H.I.M., et al., 2020a. International Federation of Clinical Neurophysiology (IFCN) - EEG research workgroup: Recommendations on frequency and topographic analysis of resting state EEG rhythms. Part 1: Applications in clinical research studies. Clin Neurophysiol Off J Int Fed Clin. Neurophysiol. 131, 285–307. https://doi.org/10.1016/j.clinph.2019.06.234.

Babiloni, C., Blinowska, K., Bonanni, L., Cichocki, A., De Haan, W., Del Percio, C., et al., 2020b. What electrophysiology tells us about Alzheimer's disease: a window into the synchronization and connectivity of brain neurons. Neurobiol. Aging 85, 58–73. https://doi.org/10.1016/j.neurobiolaging.2019.09.008.

Babiloni, C., Carducci, F., Lizio, R., Vecchio, F., Baglieri, A., Bernardini, S., et al., 2013. Resting state cortical electroencephalographic rhythms are related to gray matter volume in subjects with mild cognitive impairment and Alzheimer's disease. Hum. Brain Mapp. 34, 1427–1446. https://doi.org/10.1002/hbm.22005.

Babiloni, C., Del Percio, C., Boccardi, M., Lizio, R., Lopez, S., Carducci, F., et al., 2015. Occipital sources of resting-state alpha rhythms are related to local gray matter density in subjects with amnesic mild cognitive impairment and Alzheimer's disease. Neurobiol. Aging 36, 556–570. https://doi.org/10.1016/j.neurobiolaging.2014.09.011.

Babiloni, C., Del Percio, C., Caroli, A., Salvatore, E., Nicolai, E., Marzano, N., et al., 2016. Cortical sources of resting state EEG rhythms are related to brain hypometabolism in subjects with Alzheimer's disease: an EEG-PET study. Neurobiol. Aging 48, 122–134. https://doi.org/10.1016/j.neurobiolaging.2016.08.021.

Babiloni, C., Del Percio, C., Lizio, R., Noce, G., Cordone, S., Lopez, S., et al., 2017. Abnormalities of cortical neural synchronization mechanisms in patients with dementia due to Alzheimer's and Lewy body diseases: an EEG study. Neurobiol. Aging 55, 143–158. https://doi.org/10.1016/j.neurobiolaging.2017.03.030.

Babiloni, C., Del Percio, C., Lizio, R., Noce, G., Lopez, S., Soricelli, A., et al., 2018a. Abnormalities of resting state cortical EEG rhythms in subjects with mild cognitive impairment due to Alzheimer's and Lewy body diseases. J Alzheimers Dis JAD 62, 247–268. https://doi.org/10.3233/JAD-170703.

Babiloni, C., Del Percio, C., Lizio, R., Noce, G., Lopez, S., Soricelli, A., et al., 2018b. Abnormalities of resting-state functional cortical connectivity in patients with dementia due to Alzheimer's and Lewy body diseases: an EEG study. Neurobiol. Aging 65, 18–40. https://doi.org/10.1016/j.neurobiolaging.2017.12.023.

Babiloni, C., Ferri, R., Noce, G., Lizio, R., Lopez, S., Lorenzo, I., et al., 2021a. Abnormalities of cortical sources of resting state alpha electroencephalographic rhythms are related to education attainment in cognitively unimpaired seniors and patients with Alzheimer's disease and amnesic mild cognitive impairment. Cereb Cortex N Y N 1991 (31), 2220–2237. https://doi.org/10.1093/cercor/bhaa356.

Babiloni, C., Ferri, R., Noce, G., Lizio, R., Lopez, S., Lorenzo, I., et al., 2021b. resting state alpha electroencephalographic rhythms are differently related to aging in cognitively unimpaired seniors and patients with Alzheimer's disease and amnesic mild cognitive impairment. J Alzheimers Dis JAD 82, 1085–1114. https://doi.org/10.3233/JAD-201271.

Bergamino, M., Walsh, R.R., Stokes, A.M., 2021. Free-water diffusion tensor imaging improves the accuracy and sensitivity of white matter analysis in Alzheimer's disease. Sci. Rep. 11, 6990. https://doi.org/10.1038/s41598-021-86505-7.

Bernstein, A.S., Rapcsak, S.Z., Hornberger, M., Saranathan, M., 2021. Alzheimer's disease neuroimaging initiative. Structural changes in thalamic nuclei across prodromal and clinical Alzheimer's disease. J Alzheimers Dis JAD 82, 361–371. https://doi.org/10.3233/JAD-201583.

Bonanni, E., Maestri, M., Tognoni, G., Fabbrini, M., Nucciarone, B., Manca, M.L., et al., 2005. Daytime sleepiness in mild and moderate Alzheimer's disease and its relationship with cognitive impairment. J. Sleep Res. 14, 311–317. https://doi.org/10.1111/j.1365-2869.2005.00462.x.

Brueggen, K., Kasper, E., Dyrba, M., Bruno, D., Pomara, N., Ewers, M., et al., 2016. The primacy effect in amnestic mild cognitive impairment: associations with hippocampal functional connectivity. Front. Aging Neurosci. 8. https://doi.org/10.3389/fnagi.2016.00244.

Brzecka, A., Leszek, J., Ashraf, G.M., Ejma, M., Ávila-Rodriguez, M.F., Yarla, N.S., et al., 2018. Sleep disorders associated with Alzheimer's disease: a perspective. Front. Neurosci. 12, 330. https://doi.org/10.3389/fnins.2018.00330.

Cohen J. Statistical power analysis for the behavioral sciences. 2nd ed. Hillsdale, NJ: Lawrence Erlbaum Associates; 1988.

Crespo-Garcia, M., Atienza, M., Cantero, J.L., 2008. Muscle artifact removal from human sleep EEG by using independent component analysis. Ann. Biomed. Eng. 36, 467–475. https://doi.org/10.1007/s10439-008-9442-y.

Delorme, A., Makeig, S., 2004. EEGLAB: an open source toolbox for analysis of single-trial EEG dynamics including independent component analysis. J. Neurosci. Methods 134, 9–21. https://doi.org/10.1016/j.jneumeth.2003.10.009.

Ehrenberg, A.J., Kelberman, M.A., Liu, K.Y., Dahl, M.J., Weinshenker, D., Falgàs, N., et al., 2023. Priorities for research on neuromodulatory subcortical systems in Alzheimer's disease: Position paper from the NSS PIA of ISTAART. Alzheimers Dement J Alzheimers Assoc 19, 2182–2196. https://doi.org/10.1002/alz.12937.

Fan, J.M., Kudo, K., Verma, P., Ranasinghe, K.G., Morise, H., Findlay, A.M., et al., 2023. Cortical synchrony and information flow during transition from wakefulness to light non-rapid eye movement sleep. J. Neurosci. 43, 8157–8171. https://doi.org/10.1523/JNEUROSCI.0197-23.2023.

Fang, W., Le, S., Han, W., Peng-Jiao, X., Shuai, Y., Rui-Ling, Z., et al., 2023. Association between napping and cognitive impairment: a systematic review and meta-analysis. Sleep Med. 111, 146–159. https://doi.org/10.1016/j.sleep.2023.09.022.

Folstein, M.F., Folstein, S.E., McHugh, P.R., 1975. "Mini-mental state". A practical method for grading the cognitive state of patients for the clinician. J. Psychiatr. Res. 12, 189–198. https://doi.org/10.1016/0022-3956(75)90026-6.

Freedman, M., Leach, L., Kaplan, E,, Shulman, K.I., Delis, D.C., 1994. Clock drawing: A neuropsychological analysis. Oxford University Press, New York, NY, 1994.

Gilligan, T.M., Sibilia, F., Farrell, D., Lyons, D., Kennelly, S.P., Bokde, A.L.W., 2019. No relationship between fornix and cingulum degradation and within-network decreases in functional connectivity in prodromal Alzheimer's disease. PLoS One 14, e0222977. https://doi.org/10.1371/journal.pone.0222977.

Hori, T., Hayashi, M., Morikawa, T., 1994. Topographical EEG changes and the hypnagogic experience. In: Ogilvie, R.D., Harsh, J.R., editors. Sleep Onset Norm. Abnorm. Process., Washington: American Psychological Association; 1994, p. 237–53.

Jack, C.R., Andrews, J.S., Beach, T.G., Buracchio, T., Dunn, B., Graf, A., et al., 2024. Revised criteria for diagnosis and staging of Alzheimer's disease: Alzheimer's Association Workgroup. Alzheimers Dement. 20, 5143–5169. https://doi.org/10.1002/alz.13859.

Jack, C.R., Bennett, D.A., Blennow, K., Carrillo, M.C., Dunn, B., Haeberlein, S.B., et al., 2018. NIA-AA research framework: toward a biological definition of Alzheimer's disease. Alzheimers Dement J. Alzheimers Assoc. 14, 535–562. https://doi.org/10.1016/j.jalz.2018.02.018.

Jaworska, N., Blier, P., Fusee, W., Knott, V., 2012. α Power, α asymmetry and anterior cingulate cortex activity in depressed males and females. J. Psychiatr. Res. 46, 1483–1491. https://doi.org/10.1016/j.jpsychires.2012.08.003.

Jeanmonod, D., Magnin, M., Morel, A., 1996. Low-threshold calcium spike bursts in the human thalamus. Common physiopathology for sensory, motor and limbic positive symptoms. Brain. J. Neurol. 119 (Pt 2), 363–375. https://doi.org/10.1093/brain/119.2.363.

Jovicich, J., Babiloni, C., Ferrari, C., Marizzoni, M., Moretti, D.V., Del Percio, C., et al., 2019. Two-year longitudinal monitoring of amnestic mild cognitive impairment patients with prodromal Alzheimer's disease using topographical biomarkers derived from functional magnetic resonance imaging and electroencephalographic activity. J Alzheimers Dis JAD 69, 15–35. https://doi.org/10.3233/JAD-180158.

Jovicich, J., Marizzoni, M., Bosch, B., Bartrés-Faz, D., Arnold, J., Benninghoff, J., et al., 2014. Multisite longitudinal reliability of tract-based spatial statistics in diffusion tensor imaging of healthy elderly subjects. Neuroimage 101, 390–403. https://doi.org/10.1016/j.neuroimage.2014.06.075.

Jung, T.P., Makeig, S., Humphries, C., Lee, T.W., McKeown, M.J., Iragui, V., et al., 2000. Removing electroencephalographic artifacts by blind source separation. Psychophysiology 37, 163–178.

Khanna, A., Pascual-Leone, A., Michel, C.M., Farzan, F., 2015. Microstates in resting-state EEG: current status and future directions. Neurosci. Biobehav. Rev. 49, 105–113. https://doi.org/10.1016/j.neubiorev.2014.12.010.
Kitamura, K., Watanabe, Y., Nakamura, K., Takano, C., Hayashi, N., Sato, H., et al., 2021. Short daytime napping reduces the risk of cognitive decline in community-dwelling older adults: a 5-year longitudinal study. BMC Geriatr. 21, 474. https://doi.org/10.1186/s12877-021-02418-0.
Klimesch, W., 1999. EEG alpha and theta oscillations reflect cognitive and memory performance: a review and analysis. Brain Res. Brain Res. Rev. 29, 169–195. https://doi.org/10.1016/s0165-0173(98)00056-3.
Klimesch, W., 1996. Memory processes, brain oscillations and EEG synchronization. Int J Psychophysiol Off J Int Organ Psychophysiol 24, 61–100. https://doi.org/10.1016/s0167-8760(96)00057-8.
Kuhn, T., Becerra, S., Duncan, J., Spivak, N., Dang, B.H., Habelhah, B., et al., 2021. Translating state-of-the-art brain magnetic resonance imaging (MRI) techniques into clinical practice: multimodal MRI differentiates dementia subtypes in a traditional clinical setting. Quant. Imaging Med. Surg. 11, 4056–4073. https://doi.org/10.21037/qims-20-1355.
Lancini, E., Haag, L., Bartl, F., Rühling, M., Ashton, N.J., Zetterberg, H., et al., 2023. Cerebrospinal fluid and positron-emission tomography biomarkers for noradrenergic dysfunction in neurodegenerative diseases: a systematic review and meta-analysis. Brain Commun 5, fcad085. https://doi.org/10.1093/braincomms/fcad085.
Lehmann, D., Ozaki, H., Pal, I., 1987. EEG alpha map series: brain micro-states by space-oriented adaptive segmentation. Electroencephalogr. Clin. Neurophysiol. 67, 271–288. https://doi.org/10.1016/0013-4694(87)90025-3.
Leng, Y., Redline, S., Stone, K.L., Ancoli-Israel, S., Yaffe, K., 2019. Objective napping, cognitive decline, and risk of cognitive impairment in older men. Alzheimers Dement J Alzheimers Assoc 15, 1039–1047. https://doi.org/10.1016/j.jalz.2019.04.009.
Li, P., Gao, L., Yu, L., Zheng, X., Ulsa, M.C., Yang, H.-W., et al., 2023. Daytime napping and Alzheimer's dementia: a potential bidirectional relationship. Alzheimers Dement J Alzheimers Assoc 19, 158–168. https://doi.org/10.1002/alz.12636.
Lim, A.S.P., Kowgier, M., Yu, L., Buchman, A.S., Bennett, D.A., 2013. Sleep fragmentation and the risk of incident Alzheimer's disease and cognitive decline in older persons. Sleep 36, 1027–1032. https://doi.org/10.5665/sleep.2802.
Lim, M.M., Gerstner, J.R., Holtzman, D.M., 2014. The sleep-wake cycle and Alzheimer's disease: what do we know? Neurodegener Dis Manag 4, 351–362. https://doi.org/10.2217/nmt.14.33.
Liu, Q., Ganzetti, M., Wenderoth, N., Mantini, D., 2018. Detecting large-scale brain networks using EEG: impact of electrode density, head modeling and source localization. Front Neuroinformatics 12, 4. https://doi.org/10.3389/fninf.2018.00004.
Llinás, R.R., Steriade, M., 2006. Bursting of thalamic neurons and states of vigilance. J. Neurophysiol. 95, 3297–3308. https://doi.org/10.1152/jn.00166.2006.
Losert, A., Sander, C., Schredl, M., Heilmann-Etzbach, I., Deuschle, M., Hegerl, U., et al., 2020. Enhanced vigilance stability during daytime in insomnia disorder. Brain Sci. 10, 830. https://doi.org/10.3390/brainsci10110830.
Lovato, N., Lack, L., 2010. The effects of napping on cognitive functioning. Prog. Brain Res. 185, 155–166. https://doi.org/10.1016/B978-0-444-53702-7.00009-9.
Marino, M., Liu, Q., Brem, S., Wenderoth, N., Mantini, D., 2016. Automated detection and labeling of high-density EEG electrodes from structural MR images. J. Neural Eng. 13, 056003. https://doi.org/10.1088/1741-2560/13/5/056003.
Marizzoni, M., Ferrari, C., Babiloni, C., Albani, D., Barkhof, F., Cavaliere, L., et al., 2020. CSF cutoffs for MCI due to AD depend on APOEε4 carrier status. Neurobiol. Aging 89, 55–62. https://doi.org/10.1016/j.neurobiolaging.2019.12.019.
Mattsson, N., 2011. CSF biomarkers in neurodegenerative diseases. Clin. Chem. Lab. Med. 49, 345–352. https://doi.org/10.1515/CCLM.2011.082.
Mayo, C.D., Mazerolle, E.L., Ritchie, L., Fisk, J.D., Gawryluk, J.R., 2017. Alzheimer's Disease neuroimaging initiative. Longitudinal changes in microstructural white matter metrics in Alzheimer's disease. NeuroImage Clin 13, 330–338. https://doi.org/10.1016/j.nicl.2016.12.012.
Michel, C.M., Brunet, D., 2019. EEG source imaging: a practical review of the analysis steps. Front. Neurol. 10, 325. https://doi.org/10.3389/fneur.2019.00325.
Michel, C.M., Koenig, T., 2018. EEG microstates as a tool for studying the temporal dynamics of whole-brain neuronal networks: a review. Neuroimage 180, 577–593. https://doi.org/10.1016/j.neuroimage.2017.11.062.
Moran, M., Lynch, C.A., Walsh, C., Coen, R., Coakley, D., Lawlor, B.A., 2005. Sleep disturbance in mild to moderate Alzheimer's disease. Sleep Med. 6, 347–352. https://doi.org/10.1016/j.sleep.2004.12.005.
Morris, J.C., 1993. The clinical dementia rating (CDR): current version and scoring rules. Neurology 43, 2412–2414. https://doi.org/10.1212/wnl.43.11.2412-a.
van de Mortel, L.A., Thomas, R.M., van Wingen, G.A., 2021. Alzheimer's disease neuroimaging initiative. Grey matter loss at different stages of cognitive decline: A role for the thalamus in developing Alzheimer's disease. J Alzheimers Dis JAD 83, 705–720. https://doi.org/10.3233/JAD-210173.
Nabizadeh, F., Balabandian, M., Rostami, M.R., Kankam, S.B., Ranjbaran, F., Pourhamzeh, M., et al., 2022. Plasma neurofilament light levels correlate with white matter damage prior to Alzheimer's disease: results from ADNI. Aging Clin. Exp. Res. 34, 2363–2372. https://doi.org/10.1007/s40520-022-02095-y.
Nakaizumi, K., Ouchi, Y., Terada, T., Yoshikawa, E., Kakimoto, A., Isobe, T., et al., 2018. In vivo depiction of α7 nicotinic receptor loss for cognitive decline in Alzheimer's disease. J Alzheimers Dis JAD 61, 1355–1365. https://doi.org/10.3233/JAD-170591.
Novelli G, Papagno C, Capitani E, Laiacona M, et al. Tre test clinici di memoria verbale a lungo termine: Taratura su soggetti normali. [Three clinical tests for the assessment of verbal long-term memory function: Norms from 320 normal subjects.]. Arch Psicol Neurol Psichiatr 1986;47:278–96.
Oh, J.Y., Eser, R.A., Ehrenberg, A.J., Morales, D., Petersen, C., Kudlacek, J., et al., 2019. Profound degeneration of wake-promoting neurons in Alzheimer's disease. Alzheimers Dement J Alzheimers Assoc 15, 1253–1263. https://doi.org/10.1016/j.jalz.2019.06.3916.
Oh, J.Y., Walsh, C.M., Ranasinghe, K., Mladinov, M., Pereira, F.L., Petersen, C., et al., 2022. Subcortical neuronal correlates of sleep in neurodegenerative diseases. JAMA Neurol. 79, 498. https://doi.org/10.1001/jamaneurol.2022.0429.
Oken, B.S., Salinsky, M.C., Elsas, S.M., 2006. Vigilance, alertness, or sustained attention: physiological basis and measurement. Clin Neurophysiol Off J Int Fed Clin Neurophysiol 117, 1885–1901. https://doi.org/10.1016/j.clinph.2006.01.017.
Pengsuwankasem, N., Sittiprapaporn, P., Rattanabun, W., Sangmanee, N., Wongsuphasawat, K., Rintra, J., et al., 2023. The effect of short daytime napping on cognitive function, sleep quality, and quality of life in mild cognitive impairment patients. Neurosci. Lett. 817, 137499. https://doi.org/10.1016/j.neulet.2023.137499.
Peter-Derex, L., Yammine, P., Bastuji, H., Croisile, B., 2015. Sleep and Alzheimer's disease. Sleep Med. Rev. 19, 29–38. https://doi.org/10.1016/j.smrv.2014.03.007.
Prokopiou, P.C., Engels-Domínguez, N., Schultz, A.P., Sepulcre, J., Koops, E.A., Papp, K. V., et al., 2023. Association of novelty-related locus coeruleus function with entorhinal tau deposition and memory decline in preclinical Alzheimer disease. Neurology 101, e1206–e1217. https://doi.org/10.1212/WNL.0000000000207646.
Qiu, T., Zeng, Q., Zhang, Y., Luo, X., Xu, X., Li, X., et al., 2022. Altered functional connectivity pattern of hippocampal subfields in individuals with objectively-defined subtle cognitive decline and its association with cognition and cerebrospinal fluid biomarkers. Eur. J. Neurosci. 56, 6227–6238. https://doi.org/10.1111/ejn.15860.
Pascual-Marqui, R.D., 2007. Discrete, 3D distributed, linear imaging methods of electric neuronal activity. Part 1: exact, zero error localization. Doi: 10.48550/ARXIV.0710.3341.
Reitan RM, Wolfson D. The Halstead-Reitan Neuropsychological Test Battery. Tucson, AZ: Neuropsychology Press; 1985.
Richter, N., Nellessen, N., Dronse, J., Dillen, K., Jacobs, H.I.L., Langen, K.-J., et al., 2019. Spatial distributions of cholinergic impairment and neuronal hypometabolism differ in MCI due to AD. NeuroImage Clin 24, 101978. https://doi.org/10.1016/j.nicl.2019.101978.
Rosen, W.G., Mohs, R.C., Davis, K.L., 1984. A new rating scale for Alzheimer's disease. Am. J. Psychiatry 141, 1356–1364. https://doi.org/10.1176/ajp.141.11.1356.
Rosen, W.G., Terry, R.D., Fuld, P.A., Katzman, R., Peck, A., 1980. Pathological verification of ischemic score in differentiation of dementias. Ann. Neurol. 7, 486–488. https://doi.org/10.1002/ana.410070516.
Rossini, P.M., Di Iorio, R., Vecchio, F., Anfossi, M., Babiloni, C., Bozzali, M., et al., 2020. Early diagnosis of Alzheimer's disease: the role of biomarkers including advanced EEG signal analysis. Report from the IFCN-sponsored panel of experts. Clin Neurophysiol Off J Int Fed Clin. Neurophysiol. 131, 1287–1310. https://doi.org/10.1016/j.clinph.2020.03.003.
Sabri, O., Meyer, P.M., Gräf, S., Hesse, S., Wilke, S., Becker, G.-A., et al., 2018. Cognitive correlates of α4β2 nicotinic acetylcholine receptors in mild Alzheimer's dementia. Brain J. Neurol. 141, 1840–1854. https://doi.org/10.1093/brain/awy099.
Schmidt, F.M., Sander, C., Dietz, M.-E., Nowak, C., Schröder, T., Mergl, R., et al., 2017. Brain arousal regulation as response predictor for antidepressant therapy in major depression. Sci. Rep. 7, 45187. https://doi.org/10.1038/srep45187.
Schmidt, M., 1996. Rey Auditory verbal learning test: A handbook. Los Angeles, CA: Western Psychological Services; 1996.
Setiadi, T.M., Martens, S., Opmeer, E.M., Marsman, J.-B.-C., Tumati, S., Reesink, F.E., et al., 2021. Widespread white matter aberration is associated with the severity of apathy in amnestic Mild Cognitive Impairment: Tract-based spatial statistics analysis. NeuroImage Clin. https://doi.org/10.1016/j.nicl.2021.102567.
Shan, L., Bossers, K., Unmehopa, U., Bao, A.-M., Swaab, D.F., 2012. Alterations in the histaminergic system in Alzheimer's disease: a postmortem study. Neurobiol. Aging 33, 2585–2598. https://doi.org/10.1016/j.neurobiolaging.2011.12.026.
Singh, N.A., Goodrich, A.W., Graff-Radford, J., Machulda, M.M., Sintini, I., Carlos, A.F., et al., 2024. Altered structural and functional connectivity in posterior cortical atrophy and dementia with lewy bodies. Neuroimage 290, 120564. https://doi.org/10.1016/j.neuroimage.2024.120564.
Smith, S.M., Jenkinson, M., Johansen-Berg, H., Rueckert, D., Nichols, T.E., Mackay, C.E., et al., 2006. Tract-based spatial statistics: voxelwise analysis of multi-subject diffusion data. Neuroimage 31, 1487–1505. https://doi.org/10.1016/j.neuroimage.2006.02.024.
Sultzer, D.L., Lim, A.C., Gordon, H.L., Yarns, B.C., Melrose, R.J., 2022. Cholinergic receptor binding in unimpaired older adults, mild cognitive impairment, and Alzheimer's disease dementia. Alzheimers Res. Ther. 14, 25. https://doi.org/10.1186/s13195-021-00954-w.
Tang, F., Zhu, D., Ma, W., Yao, Q., Li, Q., Shi, J., 2021. Differences changes in cerebellar functional connectivity between mild cognitive impairment and Alzheimer's disease: a seed-based approach. Front. Neurol. 12, 645171. https://doi.org/10.3389/fneur.2021.645171.
Ulke, C., Wittekind, D.A., Spada, J., Franik, K., Jawinski, P., Hensch, T., et al., 2019. Brain arousal regulation in SSRI-medicated patients with major depression. J. Psychiatr. Res. 108, 34–39. https://doi.org/10.1016/j.jpsychires.2018.11.003.
Velioglu, H.A., Ayyildiz, B., Ayyildiz, S., Sutcubasi, B., Hanoglu, L., Bayraktaroglu, Z., et al., 2023. A structural and resting-state functional connectivity investigation of the pulvinar in elderly individuals and Alzheimer's disease patients. Alzheimers Dement. 19, 2774–2789. https://doi.org/10.1002/alz.12850.
Wang, J., Wang, P., Jiang, Y., Wang, Z., Zhang, H., Li, H., et al., 2022. Hippocampus-based dynamic functional connectivity mapping in the early stages of Alzheimer's

disease. J Alzheimers Dis JAD 85, 1795–1806. https://doi.org/10.3233/JAD-215239.
Wechsler D. WMS-R: Wechsler Memory Scale-Revised: Manual. San Antonio, TX: Psychological Corporation; 1987.
Wen, Q., Mustafi, S.M., Li, J., Risacher, S.L., Tallman, E., Brown, S.A., et al., 2019. White matter alterations in early-stage Alzheimer's disease: a tract-specific study. Alzheimers Dement Amst Neth 11, 576–587. https://doi.org/10.1016/j.dadm.2019.06.003.
Wu, Y., Wu, X., Gao, L., Yan, Y., Geng, Z., Zhou, S., et al., 2022. Abnormal functional connectivity of thalamic subdivisions in Alzheimer's disease: a functional magnetic resonance imaging study. Neuroscience 496, 73–82. https://doi.org/10.1016/j.neuroscience.2022.06.006.
Xia, Y., Eeles, E., Fripp, J., Pinsker, D., Thomas, P., Latter, M., et al., 2022. Reduced cortical cholinergic innervation measured using [18F]-FEOBV PET imaging correlates with cognitive decline in mild cognitive impairment. NeuroImage Clin 34, 102992. https://doi.org/10.1016/j.nicl.2022.102992.
Xiao, D., Wang, K., Theriault, L., Charbel, E., 2022. Alzheimer's Disease Neuroimaging Initiative. White matter integrity and key structures affected in Alzheimer's disease characterized by diffusion tensor imaging. Eur. J. Neurosci. 56, 5319–5331. https://doi.org/10.1111/ejn.15815.
Yesavage, J.A., Brink, T.L., Rose, T.L., Lum, O., Huang, V., Adey, M., et al., 1982. Development and validation of a geriatric depression screening scale: a preliminary report. J. Psychiatr. Res. 17, 37–49. https://doi.org/10.1016/0022-3956(82)90033-4.
Yu, E., Liao, Z., Tan, Y., Qiu, Y., Zhu, J., Han, Z., et al., 2019. High-sensitivity neuroimaging biomarkers for the identification of amnestic mild cognitive impairment based on resting-state fMRI and a triple network model. Brain Imaging Behav. 13, 1–14. https://doi.org/10.1007/s11682-017-9727-6.
Zhao, Q., Sang, X., Metmer, H., Swati, Z.N.N.K., Lu, J., 2019. Alzheimer's disease neuroimaging initiative. Functional segregation of executive control network and frontoparietal network in Alzheimer's disease. Cortex J Devoted Study Nerv Syst Behav 120, 36–48. https://doi.org/10.1016/j.cortex.2019.04.026.
Zhong, S., Lou, J., Ma, K., Shu, Z., Chen, L., Li, C., et al., 2023. Disentangling in-vivo microstructural changes of white and gray matter in mild cognitive impairment and Alzheimer's disease: a systematic review and meta-analysis. Brain Imaging Behav. 17, 764–777. https://doi.org/10.1007/s11682-023-00805-2.
Zhu, Q.-Y., Bi, S.-W., Yao, X.-T., Ni, Z.-Y., Li, Y., Chen, B.-Y., et al., 2015. Disruption of thalamic connectivity in Alzheimer's disease: a diffusion tensor imaging study. Metab. Brain Dis. 30, 1295–1308. https://doi.org/10.1007/s11011-015-9708-7.